Production of charmed mesons in Z decays

D. Buskulic, I. De Bonis, D. Decamp, P. Ghez, C. Goy, J.P. Lees, M.N. Minard, B. Pietrzyk, F. Ariztizabal, P. Comas, et al.

AB

EUROPEAN ORGANIZATION FOR NUCLEAR RESEARCH

CERN-PPE/93-208
December 1st, 1993

Su 9401
9

Production of Charmed Mesons in Z Decays

The ALEPH Collaboration*

Abstract

The production of charmed mesons $\overset{(-)}{\mathrm{D}}{}^0$, $\mathrm{D}^{\pm}$, and $\mathrm{D}^{*\pm}$ is studied in a sample of 478,000 hadronic Z decays. The production rates are measured to be

$$\frac{\Gamma(\mathrm{Z} \to \mathrm{D}^{*\pm}\mathrm{X})}{\Gamma_{had}} = 0.187 \pm 0.015(\mathrm{exp.}) \pm 0.013(\mathrm{BR}),$$

$$\frac{\Gamma(\mathrm{Z} \to \mathrm{D}^{\pm}\mathrm{X})}{\Gamma_{had}} = 0.251 \pm 0.026(\mathrm{exp.}) \pm 0.025(\mathrm{BR}),$$

$$\frac{\Gamma(\mathrm{Z} \to \overset{(-)}{\mathrm{D}}{}^0\mathrm{X})}{\Gamma_{had}} = 0.518 \pm 0.052(\mathrm{exp.}) \pm 0.035(\mathrm{BR}),$$

where the errors from this analysis are separated from those coming from the D branching ratios (BR). The $\mathrm{D}^{*\pm}$ momentum distribution is extracted separately for $\mathrm{Z} \to \mathrm{c\bar{c}}$ and $\mathrm{Z} \to \mathrm{b\bar{b}}$ events with the help of event shape variables. It is consistent with the prediction of the JETSET Monte Carlo program after adjustment of the charm fragmentation function. Constraining the shape of the $\mathrm{Z} \to \mathrm{b\bar{b}}$ contribution, the average fraction of the beam energy taken by a D^* meson produced in the fragmentation of a charm quark is extracted by a parametric fit to be $\langle X_E \rangle_c = 0.495 \pm 0.011 \pm 0.007$. Evidence for D^{**0} ($\mathrm{D}_1(2420)^0$ and/or $\mathrm{D}_2^*(2460)^0$) production is found in the $\mathrm{D}^{*\pm}\pi^{\mp}$ channel, accounting for a fraction $(18 \pm 5 \pm 2)\%$ of all $\mathrm{D}^{*\pm}$ production. The relative production of vector and pseudoscalar mesons is discussed, together with the possible effects of D^{**} production. The c-quark forward-backward Z-pole asymmetry is determined from that of high momentum $\mathrm{D}^{*\pm}$ to be

$$A_{FB}^{0,c} = (7.7 \pm 4.4)\%.$$

(Submitted to Z. Phys. C Particles and Fields)

*See the following pages for the list of authors.

The ALEPH Collaboration

D. Buskulic, I. De Bonis, D. Decamp, P. Ghez, C. Goy, J.-P. Lees, M.-N. Minard, B. Pietrzyk
Laboratoire de Physique des Particules (LAPP), IN^{2}P^3-CNRS, 74019 Annecy-le-Vieux Cedex, France

F. Ariztizabal, P. Comas, J.M. Crespo, I. Efthymiopoulos, E. Fernandez, M. Fernandez-Bosman, V. Gaitan, Ll. Garrido,[29] T. Mattison,[30] S. Orteu, A. Pacheco, C. Padilla, A. Pascual
Institut de Fisica d'Altes Energies, Universitat Autonoma de Barcelona, 08193 Bellaterra (Barcelona), Spain[7]

D. Creanza, M. de Palma, A. Farilla, G. Iaselli, G. Maggi, N. Marinelli, S. Natali, S. Nuzzo, A. Ranieri, G. Raso, F. Romano, F. Ruggieri, G. Selvaggi, L. Silvestris, P. Tempesta, G. Zito
Dipartimento di Fisica, INFN Sezione di Bari, 70126 Bari, Italy

Y. Chai, H. Hu, D. Huang, X. Huang, J. Lin, T. Wang, Y. Xie, D. Xu, R. Xu, J. Zhang, L. Zhang, W. Zhao
Institute of High-Energy Physics, Academia Sinica, Beijing, The People's Republic of China[8]

G. Bonvicini, J. Boudreau, D. Casper, H. Drevermann, R.W. Forty, G. Ganis, C. Gay, M. Girone, R. Hagelberg, J. Harvey, J. Hilgart,[27] R. Jacobsen, B. Jost, J. Knobloch, I. Lehraus, M. Maggi, C. Markou, M. Martinez, P. Mato, H. Meinhard, A. Minten, R. Miquel, H.-G. Moser, P. Palazzi, J.R. Pater, J.A. Perlas, P. Perrodo, J.-F. Pusztaszeri, F. Ranjard, L. Rolandi, J. Rothberg,[2] T. Ruan, M. Saich, D. Schlatter, M. Schmelling, F. Sefkow,[6] W. Tejessy, I.R. Tomalin, R. Veenhof, H. Wachsmuth, S. Wasserbaech,[2] W. Wiedenmann, T. Wildish, W. Witzeling, J. Wotschack
European Laboratory for Particle Physics (CERN), 1211 Geneva 23, Switzerland

Z. Ajaltouni, M. Bardadin-Otwinowska, A. Barres, C. Boyer, A. Falvard, P. Gay, C. Guicheney, P. Henrard, J. Jousset, B. Michel, J-C. Montret, D. Pallin, P. Perret, F. Podlyski, J. Proriol, F. Saadi
Laboratoire de Physique Corpusculaire, Université Blaise Pascal, IN^{2}P^3-CNRS, Clermont-Ferrand, 63177 Aubière, France

T. Fearnley, J.B. Hansen, J.D. Hansen, J.R. Hansen, P.H. Hansen, S.D. Johnson, R. Møllerud, B.S. Nilsson[1]
Niels Bohr Institute, 2100 Copenhagen, Denmark[9]

A. Kyriakis, E. Simopoulou, I. Siotis, A. Vayaki, K. Zachariadou
Nuclear Research Center Demokritos (NRCD), Athens, Greece

J. Badier, A. Blondel, G. Bonneaud, J.C. Brient, P. Bourdon, G. Fouque, L. Passalacqua, A. Rougé, M. Rumpf, R. Tanaka, M. Verderi, H. Videau
Laboratoire de Physique Nucléaire et des Hautes Energies, Ecole Polytechnique, IN^{2}P^3-CNRS, 91128 Palaiseau Cedex, France

D.J. Candlin, M.I. Parsons, E. Veitch
Department of Physics, University of Edinburgh, Edinburgh EH9 3JZ, United Kingdom[10]

E. Focardi, L. Moneta, G. Parrini
Dipartimento di Fisica, Università di Firenze, INFN Sezione di Firenze, 50125 Firenze, Italy

M. Corden, M. Delfino,[12] C. Georgiopoulos, M. Ikeda,[6] D.E. Jaffe, D. Levinthal[15]
Supercomputer Computations Research Institute, Florida State University, Tallahassee, FL 32306-4052, USA [13,14]

A. Antonelli, G. Bencivenni, G. Bologna,[4] F. Bossi, P. Campana, G. Capon, F. Cerutti, V. Chiarella, G. Felici, P. Laurelli, G. Mannocchi,[5] F. Murtas, G.P. Murtas, M. Pepe-Altarelli, S. Salomone
Laboratori Nazionali dell'INFN (LNF-INFN), 00044 Frascati, Italy

P. Colrain, I. ten Have, J.G. Lynch, W. Maitland, W.T. Morton, C. Raine, P. Reeves, J.M. Scarr, K. Smith, M.G. Smith, A.S. Thompson, S. Thorn, R.M. Turnbull

Department of Physics and Astronomy, University of Glasgow, Glasgow G12 8QQ,United Kingdom[10]

B. Brandl, O. Braun, C. Geweniger, G. Graefe, P. Hanke, V. Hepp, C. Karger, E.E. Kluge, Y. Maumary, A. Putzer,[1] B. Rensch, A. Stahl, K. Tittel, M. Wunsch

Institut für Hochenergiephysik, Universität Heidelberg, 69120 Heidelberg, Fed. Rep. of Germany[16]

R. Beuselinck, D.M. Binnie, W. Cameron, M. Cattaneo, D.J. Colling, P.J. Dornan, J.F. Hassard, N.M. Lieske,[25] A. Moutoussi, J. Nash, S. Patton, D.G. Payne, M.J. Phillips, G. San Martin, J.K. Sedgbeer, A.G. Wright

Department of Physics, Imperial College, London SW7 2BZ, United Kingdom[10]

P. Girtler, D. Kuhn, G. Rudolph, R. Vogl

Institut für Experimentalphysik, Universität Innsbruck, 6020 Innsbruck, Austria[18]

C.K. Bowdery, T.J. Brodbeck, A.J. Finch, F. Foster, G. Hughes, D. Jackson, N.R. Keemer, M. Nuttall, A. Patel, T. Sloan, S.W. Snow, E.P. Whelan

Department of Physics, University of Lancaster, Lancaster LA1 4YB, United Kingdom[10]

A. Galla, A.M. Greene, K. Kleinknecht, J. Raab, B. Renk, H.-G. Sander, H. Schmidt, S.M. Walther, R. Wanke, B. Wolf,

Institut für Physik, Universität Mainz, 55099 Mainz, Fed. Rep. of Germany[16]

A.M. Bencheikh, C. Benchouk, A. Bonissent, D. Calvet, J. Carr, P. Coyle, C. Diaconu, J. Drinkard,[3] F. Etienne, D. Nicod, P. Payre, L. Roos, D. Rousseau, P. Schwemling, M. Talby

Centre de Physique des Particules, Faculté des Sciences de Luminy, IN^{2}P^3-CNRS, 13288 Marseille, France

S. Adlung, R. Assmann, C. Bauer, W. Blum, D. Brown, P. Cattaneo,[23] B. Dehning, H. Dietl, F. Dydak,[21] M. Frank, A.W. Halley, K. Jakobs, J. Lauber, G. Lütjens, G. Lutz, W. Männer, R. Richter, J. Schröder, A.S. Schwarz, R. Settles, H. Seywerd, U. Stierlin, U. Stiegler, R. St. Denis, G. Wolf

Max-Planck-Institut für Physik, Werner-Heisenberg-Institut, 80805 München, Fed. Rep. of Germany[16]

R. Alemany, J. Boucrot,[1] O. Callot, A. Cordier, M. Davier, L. Duflot, J.-F. Grivaz, Ph. Heusse, P. Janot, D.W. Kim,[19] F. Le Diberder, J. Lefrançois, A.-M. Lutz, G. Musolino, M.-H. Schune, J.-J. Veillet, I. Videau

Laboratoire de l'Accélérateur Linéaire, Université de Paris-Sud, IN^{2}P^3-CNRS, 91405 Orsay Cedex, France

D. Abbaneo, G. Bagliesi, G. Batignani, U. Bottigli, C. Bozzi, G. Calderini, M. Carpinelli, M.A. Ciocci, V. Ciulli, R. Dell'Orso, I. Ferrante, F. Fidecaro, L. Foà, F. Forti, A. Giassi, M.A. Giorgi, A. Gregorio, F. Ligabue, A. Lusiani, E.B. Mannelli, P.S. Marrocchesi, A. Messineo, F. Palla, G. Rizzo, G. Sanguinetti, P. Spagnolo, J. Steinberger, R. Tenchini,[1] G. Tonelli,[28] G. Triggiani, A. Valassi, C. Vannini, A. Venturi, P.G. Verdini, J. Walsh

Dipartimento di Fisica dell'Università, INFN Sezione di Pisa, e Scuola Normale Superiore, 56010 Pisa, Italy

A.P. Betteridge, Y. Gao, M.G. Green, D.L. Johnson, P.V. March, T. Medcalf, Ll.M. Mir, I.S. Quazi, J.A. Strong

Department of Physics, Royal Holloway & Bedford New College, University of London, Surrey TW20 OEX, United Kingdom[10]

V. Bertin, D.R. Botterill, R.W. Clifft, T.R. Edgecock, S. Haywood, M. Edwards, P.R. Norton, J.C. Thompson

Particle Physics Dept., Rutherford Appleton Laboratory, Chilton, Didcot, Oxon OX11 OQX, United Kingdom[10]

B. Bloch-Devaux, P. Colas, H. Duarte, S. Emery, W. Kozanecki, E. Lançon, M.C. Lemaire, E. Locci, B. Marx, P. Perez, J. Rander, J.-F. Renardy, A. Rosowsky, A. Roussarie, J.-P. Schuller, J. Schwindling, D. Si Mohand, B. Vallage

Service de Physique des Particules, DAPNIA, CE-Saclay, 91191 Gif-sur-Yvette Cedex, France[17]

R.P. Johnson, A.M. Litke, G. Taylor, J. Wear

Institute for Particle Physics, University of California at Santa Cruz, Santa Cruz, CA 95064, USA[22]

W. Babbage, C.N. Booth, C. Buttar, S. Cartwright, F. Combley, I. Dawson, L.F. Thompson

Department of Physics, University of Sheffield, Sheffield S3 7RH, United Kingdom[10]

E. Barberio,[31] A. Böhrer, S. Brandt, G. Cowan,[1] C. Grupen, G. Lutters, F. Rivera,[26] U. Schäfer, L. Smolik

Fachbereich Physik, Universität Siegen, 57068 Siegen, Fed. Rep. of Germany[16]

L. Bosisio, R. Della Marina, G. Giannini, B. Gobbo, L. Pitis, F. Ragusa[20]

Dipartimento di Fisica, Università di Trieste e INFN Sezione di Trieste, 34127 Trieste, Italy

L. Bellantoni, W. Chen, J.S. Conway,[24] Z. Feng, D.P.S. Ferguson, Y.S. Gao, J. Grahl, J.L. Harton, O.J. Hayes III, J.M. Nachtman, Y.B. Pan, Y. Saadi, M. Schmitt, I. Scott, V. Sharma, Z.H. Shi, J.D. Turk, A.M. Walsh, F.V. Weber, Sau Lan Wu, X. Wu, M. Zheng, G. Zobernig

Department of Physics, University of Wisconsin, Madison, WI 53706, USA[11]

---

[1]Now at CERN, PPE Division, 1211 Geneva 23, Switzerland.
[2]Permanent address: University of Washington, Seattle, WA 98195, USA.
[3]Now at University of California, Irvine, CA 92717, USA.
[4]Also Istituto di Fisica Generale, Università di Torino, Torino, Italy.
[5]Also Istituto di Cosmo-Geofisica del C.N.R., Torino, Italy.
[6]Now at DESY, Hamburg, Germany.
[7]Supported by CICYT, Spain.
[8]Supported by the National Science Foundation of China.
[9]Supported by the Danish Natural Science Research Council.
[10]Supported by the UK Science and Engineering Research Council.
[11]Supported by the US Department of Energy, contract DE-AC02-76ER00881.
[12]On leave from Universitat Autonoma de Barcelona, Barcelona, Spain.
[13]Supported by the US Department of Energy, contract DE-FG05-92ER40742.
[14]Supported by the US Department of Energy, contract DE-FC05-85ER250000.
[15]Present address: Lion Valley Vineyards, Cornelius, Oregon, U.S.A.
[16]Supported by the Bundesministerium für Forschung und Technologie, Fed. Rep. of Germany.
[17]Supported by the Direction des Sciences de la Matière, C.E.A.
[18]Supported by Fonds zur Förderung der wissenschaftlichen Forschung, Austria.
[19]Permanent address: Kangnung National University, Kangnung, Korea.
[20]Now at Dipartimento di Fisica, Università di Milano, Milano, Italy.
[21]Also at CERN, PPE Division, 1211 Geneva 23, Switzerland.
[22]Supported by the US Department of Energy, grant DE-FG03-92ER40689.
[23]Now at Università di Pavia, Pavia, Italy.
[24]Now at Rutgers University, Piscataway, NJ 08854, USA.
[25]Now at Oxford University, Oxford OX1 3RH, U.K.
[26]Partially supported by Colciencias, Colombia.
[27]Now at SSCL, Dallas 75237-3946, TX, U.S.A.
[28]Also at Istituto di Matematica e Fisica, Università di Sassari, Sassari, Italy.
[29]Permanent address: Dept. d'Estructura i Constituens de la Materia, Universitat de Barcelona, 08208 Barcelona, Spain.
[30]Now at SLAC, Stanford, CA 94309, U.S.A.
[31]Now at Università della Calabria, Cosenza, Italy.

1 Introduction

In hadronic Z decays charmed mesons are expected to be produced either directly from the hadronization of charm quarks in the process $Z \rightarrow c\bar{c}$ or from the decay of b hadrons produced in $Z \rightarrow b\bar{b}$ events, with an approximately equal rate. Charmed mesons originating from the first process enable measurements of the charm quark fragmentation function and forward-backward asymmetry. Understanding the relative abundance of vector and pseudoscalar L=0 meson production and the amount of heavy charmed mesons (L=1 or radial excitations) is important for several measurements in the field of heavy flavour physics, such as the separate measurements of charged and neutral B meson lifetimes[1] or the interpretation of inclusive lepton spectra[2].

This paper is an update of Ref. [3], with statistics increased to half a million Z's. The data recorded in 1991 benefitted from an improved charged track momentum resolution with the introduction of a vertex detector. Six exclusive decay channels have been studied (charge-conjugate modes are implied throughout):

(i) $D^0 \rightarrow K^-\pi^+$;
(ii) $D^{*+} \rightarrow D^0\pi^+$, followed by (i) ;
(iii) $D^+ \rightarrow K^-\pi^+\pi^+$;
(iv) $D^{**0} \rightarrow D^{*+}\pi^-$ where the D^{*+} undergoes decay chain (ii);
(v) $D^{*+} \rightarrow D^0\pi^+$, followed by $D^0 \rightarrow K^-\pi^+\pi^+\pi^-$;
(vi) $D^{*+} \rightarrow D^0\pi^+$, followed by $D^0 \rightarrow K^-\pi^+\pi^0$.

Using these channels a number of measurements have been achieved. As in Ref. [3], the cleaner decay process (ii) was used to extract the $X_E \equiv E_{meson}/E_{beam}$ spectrum of D^* mesons, but with the relative contributions from $Z \rightarrow c\bar{c}$ and $Z \rightarrow b\bar{b}$ processes now disentangled using global event shape variables. A parametric fit to these distributions leads to an estimate of the average X_E of D^* mesons produced in $Z \rightarrow c\bar{c}$ events. The dependence of the results on the choice of the parametrization of the fragmentation function was studied in detail. The comparison of the rates for $(i), (ii)$ and (iii) leads to an estimate of the vector to pseudoscalar production ratio. A search was performed for higher mass states via their decays (iv) into a charged D^* and a charged pion. The decay modes $(ii), (v)$ and (vi) were used in the measurement of the forward-backward asymmetry.

2 ALEPH Detector and Data Selection

This study uses data recorded from 1989 to 1991 by the ALEPH detector at the LEP e^+e^- storage ring. A detailed description of ALEPH can be found in Reference [4]. The features most relevant to this study are given here. The tracking uses a set of three concentric detectors: a large Time Projection Chamber (TPC) surrounding a drift chamber 57cm in diameter, called the "Inner Tracking Chamber" (ITC), and, closest to the interaction region,

a silicon vertex detector (VDET) [5]. The installation of the VDET was completed at the beginning of the 1991 period of data taking. This whole tracking system is inside a 1.5 T magnetic field produced by a superconducting solenoid. A global fit to the ITC, TPC (and VDET for 1991 data) coordinates allows the track momentum to be measured with an accuracy [4, 6, 7] of $\delta p/p = a \cdot p_{\mathrm{T}}$, where $a = 8 \cdot 10^{-4} (GeV/c)^{-1}$ in 1990 and $6 \cdot 10^{-4} (GeV/c)^{-1}$ in 1991, with 60% of the data taken in 1991. Multiple scattering contributes an additional term $\delta p/p = 0.003$.

The data sample consists of 477,918 hadronic events. These events are selected by the requirement that they contain at least five charged tracks of momentum above 0.2 GeV/c and polar angle θ, with respect to the beam axis, satisfying $|\cos\theta| \leq 0.95$, which implies that they cross at least six rows of cathode pads of the TPC. They must include at least 4 measured coordinates from the TPC and their distance of closest approach to the interaction vertex must be less than 10 cm along the beam axis and less than 2 cm in the transverse plane. The sum of the momenta of all tracks meeting these conditions must be greater than 10% of the centre-of-mass energy. This selects hadronic Z decays with an efficiency of 97.4±0.3%, leaving a contribution of 0.7±0.1% from τ pairs and two-photon scattering [8]. The efficiency is flavour-independent except for $\mathrm{b\bar{b}}$ events (98.0%).

Most of the data were taken at the Z peak energy; the remainder was at 1, 2, or 3 GeV above or below the peak. The use of reduced quantities (energies divided by the beam energy) allows all the data to be combined for the measurement of quantities which are not expected to depend strongly on the beam energy, e.g. fragmentation parameters.

3 The Monte Carlo Model

A Monte Carlo model including initial state radiation is used to estimate the selection efficiencies, to parametrize the heavy-quark fragmentation and to give guidance on the background composition and shape. The jets are simulated according to the JETSET parton shower evolution and fragmentation [9]. The light-quark fragmentation and QCD parameters were optimized to fit ALEPH data [10]. For heavy quarks Q = b, c, the Peterson *et al.* fragmentation function [11] is used

$$f(z) \propto z^{-1} \left(1 - \frac{1}{z} - \frac{\varepsilon_Q}{(1-z)}\right)^{-2} , \qquad (1)$$

where z is the fraction of $(E + p_{\|})$ of the meson relative to the parent quark and ε_Q is a parameter giving the 'hardness' of the energy spectrum. The value of $\varepsilon_b = (4.9 \pm 0.6) \times 10^{-3}$, has been obtained from a fit to the momentum spectrum of leptons in hadronic events [12]. The determination of ε_c is one aim of this study. The exact value of z used in the generation of the heavy hadron momenta is kept on each simulated event record in order to obtain the spectra for any value of the ε_Q parameters by event weighting. Other parametrizations such as the function of Kartvelishvili *et al.*[13] and the model of Collins and Spiller [14] have been implemented in order to assess the stability of the results under changes of the fragmentation function. The fragmentation parameters are correlated with the QCD parameters modelling the gluon emission. The ε_Q values quoted in this paper correspond to the QCD parameters of Ref. [10].

The decay parameters of c- and b-hadrons were tuned to reproduce the latest measurements. Of particular importance is the momentum distribution of D mesons produced in b-hadron decays. The model used reproduces recent data[15] on the X_E distribution of D^0's produced in B decays with a precision of better than 2% on the average momentum.

Charmed meson production is simulated as follows. In $Z \rightarrow c\bar{c}$ decays, 12% of the charm quarks fragment into a $D_s^{\pm}$, 8% into a baryon and, apart from a small production of charmonium states at the 1% level, the remainder into vector and pseudoscalar L=0 states (D^*'s and D's) with relative probabilities of 3 to 1 according to the number of spin degrees of freedom. No other kind of charmed mesons are produced by this generator. A fraction of 2% of the charmed mesons originate from charm quarks produced through the gluon splitting process $g \rightarrow c\bar{c}$. They are at low momentum. The breakdown for $Z \rightarrow b\bar{b}$ is similar, with a $D_s^{\pm}$ contribution enhanced to 15% by the process where the virtual W from the weak decay of the b produces a $c\bar{s}$ pair. For the search for L=1 mesons (D_1^0 and D_2^{*0}) a specific generation of events containing these states has been performed.

A detailed simulation of the ALEPH detector was carried out on all the generated events. They were then processed using the standard ALEPH reconstruction program.

4 Charmed Meson Production Rates and c-quark Hadronization

4.1 Search for D^0, D^{*+}, and D^+ Decays

In this section, the selection of charmed-meson samples is described. The results will be summarized in Table 1.

4.1.1 $D^0 \rightarrow K^-\pi^+$

All pairs of oppositely charged tracks meeting the requirements of Section 2 are used to form both a D^0 and a $\bar{D}^0$ candidate by assigning the kaon mass to one of the particles and the pion mass to the other. A combination is retained if the angle θ_K^* between the K and the line of flight of the $K\pi$ system, evaluated in the $K\pi$ centre of mass, satisfies $|\cos\theta_K^*| \leq 0.8$. This rejects most of the combinatorial background, which peaks at $|\cos\theta_K^*| = 1$, while it accepts 80% of the signal since the decay of the D^0 meson is isotropic. The $K\pi$ mass distribution for candidates with $X_E > 0.25$ is shown in Fig. 1, where a clear enhancement in the D^0 mass region is visible. The mass range from 1.835 to 1.895 GeV/c^2 is used to define the D^0 sample.

Particle identification is not used for rejecting combinations. The fact that both mass assignments $K^+\pi^-$ and $K^-\pi^+$ can satisfy all the criteria leads to a certain amount of double counting. This is taken into account and was estimated by the Monte Carlo simulation to increase the signal by 20%. The background is found to contain both a 'charm' and a 'combinatorial' contribution. Monte Carlo studies show that the 'charm' contribution is due to charmed mesons (D^0, $D^{\pm}$, and D_s) decaying into two charged particles plus others, neutral or charged. The 'combinatorial' background is fitted with a third-degree polynomial, which agrees with the Monte Carlo prediction for the light quark contribution. These two contributions are also shown in Fig. 1. Subtracting the background in the signal region and correcting for double-counting leads to a signal of $3719 \pm 138(stat.) \pm 152(syst.)$ D^0's

with X_E >0.25. The systematic error comes from the background subtraction. It has been estimated by varying the fit range and the shape of the combinatorial background.

4.1.2 $D^{*+} \rightarrow D^0\pi_s^+$, followed by $D^0 \rightarrow K^-\pi^+$

For the $D^{*\pm}$ search one more track, the soft pion (π_s), is added to a D^0 candidate selected as described previously. The momentum of the soft pion must lie within the kinematically allowed range for a $D^{*+} \rightarrow D^0\pi_s^+$ decay with $0.25 \leq X_E(D^*) \leq 1$, i.e. 0.55 to 4.2 GeV/$c$. Here the mass assignment is unambiguous as the charge of the K must be opposite to that of the soft pion. All the cuts are the same as for process (i) except that here X_E refers to the D^* instead of the D^0. The distribution of the mass difference $\Delta M = M(K\pi\pi_s) - M(K\pi)$ is a clear signature of D^* production (Fig. 2). The simultaneous $K\pi$ mass and mass-difference (0.1435 GeV/c^2 < ΔM < 0.1475 GeV/c^2) cuts select 1090 candidates. An event at high X_E is shown in Fig. 3.

To estimate the background size and its X_E dependence an event mixing technique is used. The pions are taken from one event and the kaon is taken from another. The jet containing the kaon is then rotated so as to make its axis coincide with that of the jet of the pions. The number of background events within the cuts is estimated from the mass-difference spectrum. The shape of the background is taken from the event mixing and normalized to the data in the upper side band defined by $\Delta M \geq 0.152$ GeV/c^2. Its integral in the peak region is then taken as the number of expected background combinations. This leads to an estimate of 198 $\pm$ 5 background events. The quoted uncertainty comes from the statistical fluctuations on the background normalization. From the spread between the various fits the systematic uncertainty on the expected number of background events is estimated to be also $\pm$5.

The selection efficiency has been evaluated with the Monte Carlo to be 58% for X_E >0.25. The uncertainty on the efficiency of the mass cuts has been evaluated by using a parametrization (the sum of two gaussians) fitted to the data and varying the width and average between two extreme values compatible within $\pm 1\sigma$ with the data. As a result, the global relative error on the efficiency is found to be $\delta\epsilon/\epsilon = \pm 0.036$ for 1990 data, of which $\pm$0.025 comes from each of the two mass cuts, and $\pm$0.016 for 1991 data, of which $\pm$0.009 is for the mass-difference cut and $\pm$0.013 for the 2-body mass cut. This improvement in accuracy is a consequence of the better mass resolution from the introduction of the vertex detector.

4.1.3 $D^+ \rightarrow K^-\pi^+\pi^+$

A signal of D^+ to $K^-\pi^+\pi^+$ is seen in the invariant mass distribution of three tracks, two of them of the same sign and given a pion mass, and the third one of the opposite sign and given a kaon mass. Cuts are applied to reduce the very high combinatorial background: the D^+ reduced energy is required to be $X_E > 0.3$, and the angle α between the sphericity axis of the three tracks and the line of flight of the D^+ in its rest frame, has to satisfy $|\cos\alpha| < 0.8$. The distribution of cosα is uniform for the signal, even if the decay proceeds through $K^{*0}\pi$, and strongly peaked near $\pm$1 for the background. The signal (Fig. 4) is sought in the range from 1.84 to 1.9 GeV/c^2. It was checked on Monte Carlo events that no reflection of other

charmed hadron decays is expected to contribute significantly in the considered region of the mass distribution. The background is estimated from a polynomial fit. The number of decays after background subtraction is 3187 ± 306.

Channel	Candidates	Estimated Background	Signal	X_E cut
$D^0 \to K^-\pi^+$	27499	23780 ± 150	3719 ± 205	0.25
$D^{*+} \to D^0\pi_s^+, D^0 \to K^-\pi^+$	1090	198 ± 5	892 ± 33	0.25
$D^+ \to K^-\pi^+\pi^+$	93716	90529 ± 306	3187 ± 306	0.30

Table 1: Summary table for studied charmed meson channels.

The selection efficiency was estimated by a Monte Carlo simulation to be $(53 \pm 2)\%$, almost independent of X_E, for $X_E > 0.2$. The efficiency of the X_E cut ($X_E > 0.3$) was estimated to be $(65.1 \pm 1.4)\%$, assuming that the directly produced D^+'s follow the same X_E distribution as the D^*'s and assuming that 50% of the D^+'s are directly produced, with the other 50% coming from a D^* decay. The fit of the $D^{*\pm}$ spectrum obtained in the next section is used. The main uncertainty on this extrapolation comes from the relative normalization of the b and c contributions. The error on this ratio has been taken to be $\pm 17\%$ as a result of the $D^{*\pm}$ analysis described in the next section. The overall efficiency attached to this D^+ search is thus $(34.5 \pm 1.7)\%$.

4.2 The D* Energy Distribution

In this section, the energy distribution of the D^*'s is used to gain insight on the production mechanism. Firstly, the two expected contributions from $b\bar{b}$ and $c\bar{c}$ events are separated using global event shape variables. Then, a fit to the fully inclusive D^* distribution with a modelling of the two spectra was carried out to obtain the charm fragmentation parameter, the production rate, and the relative magnitude of the $b\bar{b}$ and $c\bar{c}$ contributions.

The $X_E(D^*)$ spectrum was extracted from the data by subtracting the background from the observed distribution and correcting the resulting distribution for the efficiency. The differential production rate $(1/N_{had})dN/dX_E$ per hadronic Z event is given in Table 2.

A partial separation of the two heavy-flavour contributions is achieved using a topological discriminator of b from u,d,s,c events. This discriminator, hereafter called V_{NN}, is the output of an artificial neural network [16] which combines nine variables characterizing the event topology [17]. These variables are calculated for each hemisphere of the event as defined by the thrust axis. In order to avoid correlation between $X_E(D^*)$ and V_{NN}, only variables related to the hemisphere which does not contain the D^* candidate are selected to calculate the b discriminator variable. The efficiency to select a b event for a given cut on V_{NN} ($\epsilon^{data}(V_{NN})$) has been obtained from $q\bar{q}$ data, using a double-tag method [16], and compared to the Monte Carlo prediction. The maximal difference between data and Monte Carlo was found to be $(0.\hat{3} \pm 0.1)\%$.

X_E range	$(1/N_{had})dN/dX_E$
0.25 - 0.30	$(994 \pm 122) \times 10^{-5}$
0.30 - 0.35	$(886 \pm 107) \times 10^{-5}$
0.35 - 0.40	$(949 \pm 104) \times 10^{-5}$
0.40 - 0.45	$(706 \pm 86) \times 10^{-5}$
0.45 - 0.50	$(582 \pm 77) \times 10^{-5}$
0.50 - 0.55	$(717 \pm 83) \times 10^{-5}$
0.55 - 0.60	$(530 \pm 71) \times 10^{-5}$
0.60 - 0.65	$(495 \pm 71) \times 10^{-5}$
0.65 - 0.70	$(506 \pm 71) \times 10^{-5}$
0.70 - 0.75	$(355 \pm 60) \times 10^{-5}$
0.75 - 0.80	$(181 \pm 43) \times 10^{-5}$
0.80 - 0.85	$(120 \pm 37) \times 10^{-5}$
0.85 - 0.90	$(60 \pm 23) \times 10^{-5}$
0.90 - 0.95	$(29 \pm 18) \times 10^{-5}$
0.95 - 1.00	$(7 \pm 7) \times 10^{-5}$

Table 2: Measured production rate as a function of the D* reduced energy.

The X_E range from 0.25 to 1 is separated into seven bins. In each X_E bin, a linear combination of the Monte Carlo $Z \rightarrow b\bar{b}$ and $Z \rightarrow c\bar{c}$ contributions is fitted to the V_{NN} shape, giving the relative contributions of the two sources. The separation between the two flavours is seen in Fig. 5. The statistical error on the two contributions are anti-correlated to a large extent. The $b\bar{b}$ contribution calculated from the JETSET Monte Carlo program (see Section 3) is shown as a solid line. It is found to be in good agreement with the data. Also, the Peterson *et al.* fragmentation function reproduces the $c\bar{c}$ part.

To obtain a more precise estimate of the charm fragmentation function the $b \rightarrow D^*$ can be constrained by external input: the b fragmentation parameter is known from the study of high-p_T leptons[12], while the D* momentum spectrum is constrained from $\Upsilon(4S)$ experiments[15]. Therefore the $b \rightarrow D^*$ contribution given by the Monte Carlo simulation can be trusted with moderate extrapolation. This assumption is supported by the agreement of the generated $b \rightarrow D^*$ spectrum with that measured (fig. 5). As the D*'s from b decays have a lower average momentum than D*'s produced in $Z \rightarrow c\bar{c}$ events, the separation of the two quark flavours achieved with V_{NN} is enhanced when using the X_E and V_{NN} variables together.

A maximum-likelihood fit to the X_E vs. V_{NN} distribution is performed. The fit parameters are: the Peterson *et al.* parameter ε_c, the fraction of charm quarks hadronizing into $D^{*\pm}$, $P_{c \rightarrow D^{*\pm}}$, and the ratio $\frac{P_{b \rightarrow D^{*\pm}}}{P_{c \rightarrow D^{*\pm}}}$. The fitted function is:

$$\frac{d^2N}{dX_E dV_{NN}} = 2N_{had} \cdot P_{c \rightarrow D^{*\pm}} \cdot B_* \cdot B_0 \cdot \epsilon(X_E, V_{NN}) \cdot f_{HF}(X_E, V_{NN}, \varepsilon_c) + N_{BG} \cdot f_{BG}(X_E, V_{NN}) , \quad (2)$$

with $\epsilon(X_E, V_{NN})$ being the selection efficiency as a function of X_E and V_{NN}. The heavy flavour contribution is given by

$$f_{HF}(X_E, V_{NN}, \varepsilon_c) = \frac{\Gamma_{b\bar{b}}}{\Gamma_{had}} \cdot \frac{P_{b\to D^{*\pm}}}{P_{c\to D^{*\pm}}} \cdot f_b(X_E, V_{NN}) + \frac{\Gamma_{c\bar{c}}}{\Gamma_{had}} \cdot f_c(X_E, V_{NN}, \varepsilon_c) \qquad (3)$$

Probabilities f_b (f_c) for a $b \to D^{*\pm}$ ($c \to D^{*\pm}$) to be in a given bin in the (X_E,V_{NN}) plane are derived from a Monte-Carlo study. The background distribution f_{BG} is derived from data events selected on the upper side of the $K^-\pi^+$ mass distribution and passing the other analysis cuts. The background normalization is determined using an event-mixing technique, as described in Section 4.1.2. The $c\bar{c}$ and $b\bar{b}$ partial widths are fixed to their Standard Model expectations. The absolute normalization of the D^* signal is contained in the product $P_{c\to D^{*\pm}}\ B_*\ B_0$, where B_* and B_0 are respectively the branching fractions $B(D^{*+} \to D^0\pi^+)$ and $B(D^0 \to K^-\pi^+)$.

The 3-parameter fit performed in the (X_E,V_{NN}) plane, for $X_E \geq 0.25$ with 13 bins in X_E and 9 in V_{NN}, gives the following results :

$$P_{c\to D^{*\pm}} \cdot B_* \cdot B_0 = (6.5 \pm 0.5(stat.) \pm 0.2(syst.)) \times 10^{-3}, \qquad (4)$$

$$\frac{P_{b\to D^{*\pm}}}{P_{c\to D^{*\pm}}} = 0.87\,^{+0.15}_{-0.13}(stat.), \qquad (5)$$

$$\varepsilon_c = (52\,^{+13}_{-11}(stat.) \pm 1(syst.)) \times 10^{-3}. \qquad (6)$$

The χ^2 of the fit is 1.3 per degree of freedom. Background-subtracted projection plots are shown in Figure 6. Systematic errors arise from uncertainties in ε_b, modelling of b-hadron decays, background normalization and selection efficiency.

The value of ε_c quoted above depends very specifically on the particular Monte Carlo program used to generate the D^* spectrum and its parameters. Therefore it is of more general value to express the result in terms of the average fractional energy carried by a D^* in a $c\bar{c}$ event $\langle X_E(D^*)\rangle_c$. It yields

$$\langle X_E(D^*)\rangle_c = 0.495\,^{+0.010}_{-0.011}(stat.) \pm 0.007(syst.). \qquad (7)$$

The dependence on the choice of the parametrization of the c fragmentation function is also included in this systematic error. This dependence was studied by repeating the fit with other parametrizations of the c and/or b fragmentation functions [13, 14]. The model-dependence uncertainty was assessed from the spread of values obtained for the different parameters, using all available fragmentation functions. This effect is very small, all the parametrizations resulting in similar X_E shapes for D^*'s produced in Z decays.

4.3 Charmed-Meson Production Rates

From the results of the previous fit (eq. 4, 5) one can derive the acceptance-corrected $D^{*\pm}$ production rate ($\Gamma_{had} = \Gamma(Z \to \text{hadrons})$):

$$\frac{\Gamma(Z \to D^{*\pm}X)}{\Gamma_{had}} \cdot B(D^{*+} \to D^0\pi_s^+) \cdot B(D^0 \to K^-\pi^+)$$

$$= 2(\frac{\Gamma_{c\bar{c}}}{\Gamma_{had}} + \frac{P_{b\to D^{*\pm}}}{P_{c\to D^{*\pm}}}\frac{\Gamma_{b\bar{b}}}{\Gamma_{had}}) \cdot P_{c\to D^{*\pm}} \cdot B_* \cdot B_0 = (4.70 \pm 0.36 \pm 0.14) \times 10^{-3}. \quad (8)$$

The D^0 production rate is obtained by normalization to the D^* rate by first measuring the fraction of the D^0 signal where the D^0 comes from a charged D^*:

$$R_* = \frac{N(D^0 \text{ from } D^{*\pm})}{N(D^0)} = 0.248 \pm 0.013 \pm 0.014 \quad (9)$$

for $X_E(D^0) > 0.25$. This number is corrected for the efficiencies of soft pion detection and for the mass cut. The D^+ rate is obtained after correction for the efficiency given in Section 4.1.3. The D^0 and D^+ energy distributions are extrapolated down to X_E=0, assuming that they are given by the same parameters as determined for the D^*'s. The following rates are obtained:

$$\frac{\Gamma(Z \to D^{\pm}X)}{\Gamma_{had}} \cdot B(D^+ \to K^-\pi^+\pi^+) = (2.01 \pm 0.21) \cdot 10^{-2} \quad (10)$$

and

$$\frac{\Gamma(Z \to \overset{(-)}{D}{}^0 X)}{\Gamma_{had}} \times B(D^0 \to K^-\pi^+) = (1.92 \pm 0.19) \times 10^{-2} \quad (11)$$

Dividing these rates by the branching ratios ($B(D^{*+} \to D^0\pi_s^+) = (68.1 \pm 1.0 \pm 1.3)\%$ [21], $B(D^0 \to K^-\pi^+) = (3.71 \pm 0.25)\%$[22], $B(D^+ \to K^-\pi^+\pi^+) = 8.0^{+0.8}_{-0.7}\%$[22]) one obtains:

$$\frac{\Gamma(Z \to D^{*\pm}X)}{\Gamma_{had}} = 0.187 \pm 0.015 \pm 0.013(\text{BR}), \quad (12)$$

$$\frac{\Gamma(Z \to D^{\pm}X)}{\Gamma_{had}} = 0.251 \pm 0.026 \pm 0.025(\text{BR}), \quad (13)$$

$$\frac{\Gamma(Z \to \overset{(-)}{D}{}^0 X)}{\Gamma_{had}} = 0.518 \pm 0.052 \pm 0.035(\text{BR}). \quad (14)$$

The first uncertainty is internal to this analysis and is mainly statistical and the second comes from the branching ratios. These are simply the number of $D^{*\pm}, D^{\pm}$ and $\overset{(-)}{D}{}^0$ produced per hadronic Z decay. These numbers are largely uncorrelated except by the common use of the branching ratio of the D^0 into $K^-\pi^+$ for the D^* and D^0 rates.

Two consistency checks among these results are possible. Firstly, as any charmed meson ($c\bar{u}$ or $c\bar{d}$) of any spin state will end up, after one or several decays, in a neutral or charged (L=0,S=0) meson, one expects the total number of non-strange mesons produced per hadronic Z decay

$$\frac{\Gamma(Z \to D^{\pm}X) + \Gamma(Z \to \overset{(-)}{D}{}^0 X)}{\Gamma_{had}} = 0.77 \pm 0.07 \quad (15)$$

to be consistent with, or slightly lower than, the number of c-quarks produced per hadronic event $2 \cdot (1.14\frac{\Gamma_{b\bar{b}}}{\Gamma_{had}} + \frac{\Gamma_{c\bar{c}}}{\Gamma_{had}}) \approx 0.84$. The factor of 1.14 in the b decay stems from the virtual W decay contribution to charm quark production. The difference between the expected number

of c-quarks and the measured number of non-strange D mesons leaves room for $(8 \pm 8)\%$ of charm quarks fragmenting into a D_s or a charmed baryon.

Assuming that the difference between the observed D^0 and D^+ rates originates from D^* decays, and with the extra assumption that among the direct D and D^* mesons, the number of charged and neutrals are equal, the following relation must hold:

$$\Gamma(Z \to \overset{(-)}{D}{}^0 X) - \Gamma(Z \to D^{\pm} X) = 2\Gamma(Z \to D^{*\pm}) \times B_*, \tag{16}$$

where $B_* = B(D^{*+} \to D^0 \pi_s^+)$. This equality is indeed verified: the ratio of left-hand side to the right-hand side is 0.86 ± 0.16.

These two relations still hold if the mesons originate in the decay of higher mass states.

4.4 The Vector to Pseudoscalar Ratio

The ratio R_* of the number of D^0's from D^{*+} decays to the total number of D^0's can be used to estimate the probability P_V of producing a charmed vector meson rather than a pseudoscalar: $P_V = V/(V + P)$. Indeed, a D^0 can either be directly produced or be the decay product of a D^{*+} (with a branching fraction $B_* = 68.1 \pm 1.0 \pm 1.3\%$ [21]) or of a D^{*0} (100% branching fraction). Assuming as above that among the direct D and D^* mesons, the number of charged and neutrals are equal, the ratio R_* can be written as

$$R_* = \frac{P_V B_*}{P_V B_* + 1} \,. \tag{17}$$

The value of $R_* = 0.248 \pm 0.013 \pm 0.014$ measured as described in Section 4.3 corresponds to $P_V = 0.484 \pm 0.050 \pm 0.012$ (the first error is internal to this analysis and the second comes from the uncertainty on the branching fraction B_*). Also, from the comparison of the D^+ and D^{*+} production rates one obtains another measurement of P_V: 0.56 ± 0.07. These two measurements are averaged to

$$P_V = 0.51 \pm 0.04, \tag{18}$$

in agreement with the result published in Ref. [3]. Simple spin counting would give $P_V \simeq 0.75$. It should be emphasized, however, that the interpretation of P_V in terms of spin-counting arguments is meaningful solely in the case where D and D^* are the only charmed mesons produced. The competing production of higher mass states [23], hereafter called D^{**}'s, can affect this interpretation, as discussed in sections 4.5 and 4.6.

The sample in which P_V is measured is a mixture of 50% $b\bar{b}$ and 50% $c\bar{c}$. In principle, there is no reason for P_V to be the same for the two contributions. However, repeating the analysis for $X_E < 0.5$ (b-purity of 65%) and $X_E > 0.5$ (c-purity of 76%), the following P_V values are found: $0.469 \pm 0.061 \pm 0.011$ in the b-enriched sample and $0.505 \pm 0.090 \pm 0.012$ in the c-enriched sample. This leads to values of P_V for pure $b\bar{b}$ and $c\bar{c}$ samples:

$$P_V(b\bar{b}) = 0.44 \pm 0.12, \tag{19}$$

$$P_V(c\bar{c}) = 0.53 \pm 0.16. \tag{20}$$

These results are consistent with those reported by the DELPHI collaboration [24] and the VENUS collaboration [25].

4.5 Evidence for $D^{**0} \to D^{*+}\pi^-$ Production

Several experiments have reported evidence for heavier charmed mesons with a mass near 2.4 GeV/c^2 [23]. One, called D_1^0, is observed in its $D^{*+}\pi^-$ decay at a mass of 2.424 ± 0.006 GeV/c^2 with a width of 20^{+9}_{-6} MeV. Another, called D_2^{*0}, has a mass of 2.4594 ± 0.0022 GeV/c^2 and a width of 19 ± 7 MeV and has been observed both in the $D\pi$ and $D^*\pi$ channels. The index 1 and 2 stands for the most favoured spin assignment, and the * indicates natural parity $(-1)^J$. They are interpreted as $L = 1$ states, expected from the quark model. In this model, there are four charmed mesons with $L = 1$ and $S = 0, 1$. The four states come from the different possible combinations of spin and orbital angular momentum, yielding spin–parities $J^P = 0^+$, 1^+, 1^+ and 2^+. One of the 1^+ states comes from the spin triplet and the other from the singlet. One of the two 1^+ states can be the observed D_1^0, the other one being too wide to be observed as a resonance. Kinematically, the more probable final states for the decay of these resonances are $D^*\pi$ and $D\pi$. The 2^+ state D_2^{*0} is allowed to decay into $D^{*+}\pi^-$ or $D^+\pi^-$. In both cases, the decay products must be in a D-wave ($L = 2$) due to spin–parity conservation. Spin–parity conservation forbids the decay of the 1^+ states into $D^+\pi^-$, and of the 0^+ state into $D^{*+}\pi^-$. The decay products $D^+\pi^-$ of the 0^+ state must be in an S-wave.

A search is performed in the data for decays of the D_1^0 and D_2^{*0} into $D^{*+}\pi^-$. In this search $D^{*\pm}$ candidates are selected as described above and paired with another charged track assumed to be a pion. The reduced energy $X_E(D^{**})$ of the D^{**} candidate is required to be larger than 0.25. To further reduce the combinatorial background, a kinematic fit of the track momenta to the D^* mass is performed and the χ^2 of this fit is required to be smaller than 7. For a combination to be kept, all the tracks are required to have the dE/dx measurement available and within two standard deviations from the mass hypothesis. The invariant mass distribution is shown in Fig. 7. The experimental resolution on the effective mass is estimated to be 6 MeV and the natural widths of the resonances have been measured to be about 20 MeV. Thus, an unbinned maximum likelihood fit to this distribution is performed using the sum of two Breit-Wigners (corresponding to D_2^{*0} and D_1^0) for the signal and a polynomial is used to parametrize the background. The masses and widths are constrained to the world average [22]. The ratio of the two Breit-Wigner distributions is: $N(D_1^0)/(N(D_1^0)+N(D_2^{*0})) = 0.30^{+0.18+0.07}_{-0.19-0.04}$. The total area is measured to be 63 ± 16 events, with a systematic uncertainty on this number of $^{+3}_{-5}$ obtained by varying the masses within errors and trying various parametrizations of the background.

Correcting this number for an overall efficiency of $(13.2 \pm 1.5)\%$ leads to the result:

$$\frac{\Gamma(Z \to D^{**0}X)}{\Gamma_{had}} \cdot B(D^{**0} \to D^{*+}\pi^-) \cdot B(D^{*+} \to D^0\pi_s^+) \cdot B(D^0 \to K^-\pi^+) = (1.02 \pm 0.26 \pm 0.14) \times 10^{-3}. \quad (21)$$

The fraction of D^{*+} originating from a D^{**0} is measured to be:

$$\frac{(D^{*+} \text{ from } D^{**0} \to D^{*+}\pi^-)}{(\text{all } D^{*+})} = (18 \pm 5 \pm 2)\%,$$

for D^{*+} with $X_E > 0.25$. The error is dominated by the uncertainty on the number of D^{**0} from the fit.

Channel	Candidates	Estimated Background	Signal
$D^{*+} \to D^0\pi_s^+, D^0 \to K^-\pi^+$	312	16 ± 1	296 ± 17.7
$D^{*+} \to D^0\pi_s^+, D^0 \to K^-\pi^+\pi^+\pi^-$	1065	400 ± 14	665 ± 36
$D^{*+} \to D^0\pi_s^+, D^0 \to K^-\pi^+\pi^0$	366	111 ± 5	255 ± 20

Table 3: Summary table for channels used in the asymmetry measurement. X_E is required to be greater than 0.5.

4.6 Implication for the Measurement of the Vector to Pseudoscalar Ratio

This observation of D^{**0} production modifies the interpretation of P_V. Depending on the exact D^{**} state produced, the ratio $B(D^{**} \to D) : B(D^{**} \to D^*)$ can vary within a large range: $2.4 \pm 0.7 : 1$ for the spin 2 state D_2^{*0} [23], $0 : 1$ for the spin 1 states D_1^0, or $1 : 0$ for the spin 0 state. Clearly, the value of P_V which is measured in Section 4.4 can be reconciled with a V/(V+P) of 0.75 for the directly produced D's and D*'s, if a substantial fraction of the D's originates from these higher mass states. This rules out the hypothesis that the D_1^0 is the only one produced, but can be arranged by a combination including the other D^{**0} states, and/or contributions from a non-resonant continuum. Note however that a value of V/(V+P) of 0.75 is not mandatory for charmed mesons coming from B decays.

5 Measurement of the $c\bar{c}$ Forward-Backward Asymmetry

In the Standard Model the production of charmed mesons in Z decays is expected to exhibit a forward-backward asymmetry. Since D*'s originating from $c\bar{c}$ events are produced at larger $\langle X_E \rangle$ than D*'s coming from $b\bar{b}$, a high purity in charm events is obtained by selecting high momentum D*'s (see Fig. 6a). The requirement $X_E \geq 0.5$ realizes a good balance between statistics and purity : 78% of the D*'s come from charm. The statistics are enhanced by using altogether the channels (ii), (v) and (vi) listed in Section 1. Though channels (v) and (vi) suffer from more background than mode (ii), they are endowed with a higher branching ratio: these 3 modes add up to about 23% of the D^0's. The number of events and the estimated background in the three channels are summarized in Table 3.

5.1 $D^{*+} \to D^0\pi_s^+$, Followed by $D^0 \to K^-\pi^+\pi^+\pi^-$

Here, the D^0 is formed using the combinations of four tracks with zero net charge. The scalar nature of the D^0 is taken advantage of in the same way as in Section 4.1.3, by cutting on the angle between the sphericity axis of the four-track system in its rest frame and the line of flight of this system. The D^0 candidate mass and the mass difference are taken in the same window as in Sections 4.1.1 and 4.1.2. It is important to keep only one of the two possible assignments of the K mass. The choice between the two assignments is not critical, as they give the same charge and direction for the quark. In case two candidates share tracks, only the one with the mass closest to the D^0 mass is kept. The mass difference distribution is shown in Fig. 8, exhibiting a clear D* signal.

channel	$D^{*+} \to D^0\pi_s^+$ $D^0 \to K^-\pi^+$	$D^{*+} \to D^0\pi_s^+$ $D^0 \to K^-\pi^+\pi^+\pi^-$	$D^{*+} \to D^0\pi_s^+$ $D^0 \to K^-\pi^+\pi^0$
Asymmetry %	-0.2±7.4	9.8±6.1	10.5±8.9
source of systematic errors %			
Background normalization	-	0.10	0.05
Background shape	0.14	1.30	0.41
b,c relative contribution	0.40	0.14	0.24
b asymmetry	0.40	0.40	0.35
χ_{mix}	0.30	0.30	0.35
χ_{D^*}	0.20	0.20	0.20
$\sum_{syst}$	0.7	1.4	0.7

Table 4: Asymmetries in the three channels with contributions to the systematic error.

A sample of 1065 candidates is selected by these cuts. A background of 400 ± 14 events is estimated by normalizing the ΔM distribution of the events with $M(K\pi\pi\pi)$ between 1.965 and 2.265 GeV/c^2 to the number of events with 0.160 GeV/$c^2 \leq \Delta M \leq$ 0.200 GeV/c^2.

5.2 $D^{*+} \to D^0\pi_s^+$, Followed by $D^0 \to K^-\pi^+\pi^0$

In this channel, the fine segmentation of the electromagnetic calorimeter is used to reconstruct the $\pi^0 \to \gamma\gamma$ decay. The energy of the photons is required to be greater than 0.5 GeV. A kinematical fit of the energies of the two photons and the angle between them to the π^0 mass is performed. Monte-Carlo simulation shows that this improves the resolution on the π^0 momentum by a factor of 2. The χ^2 probability of this fit is required to be greater than 5%. The $K\pi\pi^0$ mass distribution is shown in Fig. 9. This effective mass is required to be between 1.815 and 1.915 GeV/c^2. This selection results in a sample of 366 candidates, with a background of 111 ± 5 events estimated by the same method as in the previous section.

5.3 Fit to the Signed Angular Distribution

The signed angular distribution of the D^* mesons provides an estimate of the quark angular distribution, parametrized as:

$$\frac{1}{N^q}\frac{dN^q}{\cos\theta_q} = \frac{3}{8}(1+\cos^2\theta_q) + A_{FB}^q \cos\theta_q, \tag{22}$$

with $\cos\theta_q = Q \times \cos\theta_{D^*}$, where Q and $\cos\theta_{D^*}$ are the charge and direction of the D^* meson.

The c quark forward-backward asymmetry is measured by a maximum-likelihood fit in the $(X_E, \cos\theta_{D^*})$ plane for the three channels. To extract the Z peak asymmetry, a restricted centre-of-mass energy window of 1 GeV around the Z peak is used.

The observed $\cos\theta_{D^*}$ distribution, for each channel, can be written as the sum of three contributions :

- a background contribution, whose abundance and shape is taken from data upper side band candidates.

- a beauty contribution. The ALEPH measurement : $A_{FB}^{b} = (8.3 \pm 1.9)\%$ [12] was used to obtain the b quark asymmetry in our sample. This asymmetry is diluted, on one hand by the $B^0 - \bar{B}^0$ mixing, and by b decays producing a D^{*-} through the W on the other hand. The effective b asymmetry can be expressed as the true b asymmetry corrected by two dilution factors depending on parameters χ_{mix} and $\chi_{D^{*-}}$:

$$A_{FB}^{b,eff} = A_{FB}^{b} \times (1 - 2\chi_{mix}) \times (1 - 2\chi_{D^{*-}}). \tag{23}$$

The value of χ_{mix} is deduced from the D^* production rates through $\bar{B}_d^0$ and $\bar{B}_s^0$ mesons, together with their associated mixing parameter :

$$\chi_{mix} = f_d \chi_d + f_s \chi_s, \tag{24}$$

where the fractions f_d and f_s are taken from the Monte Carlo estimation; CLEO and ARGUS measurements of χ_d [26] are used together with ALEPH b mixing value [27] to estimate χ_s [1]. The Monte Carlo prediction $\chi_{D^{*-}} = 8\%$ is assumed with a relative uncertainty of 100%.

- a charm contribution.

The relative abundance of charm and beauty in the D^* signal is taken from the Monte Carlo together with previously fitted values of ε_c and $\frac{P_{b\to D^{*\pm}}}{P_{c\to D^{*\pm}}}$. Table 4 summarizes the results obtained on A_{FB}^{c} with statistical and systematic errors, from a fit of each of the three channels $(ii), (v)$ and (vi). The main contributions to systematics arise from asymmetries of b ($A_{FB}^{b,eff}$) and combinatorial background, and the relative abundance of the three contributions in the samples.

A simultaneous fit yields:

$$A_{FB}^{c} = (6.8 \pm 4.2(\text{stat.}) \pm 0.9(\text{syst.}))\% \tag{25}$$

Figure 10 shows the combined angular distribution after background subtraction and efficiency correction, with the result of the fit.

The MIZA program [28] is used to calculate all the corrections needed to extract the pole asymmetry and the effective electroweak mixing angle $\sin^2\theta_W^{eff}$ from our measurement. The QCD correction includes the second order calculation of Ref. [29]. Table 5 summarizes the various corrections derived using MIZA, giving

$$A_{FB}^{0,c} = (7.7 \pm 4.4)\%$$

and $\sin^2\theta_W^{eff} = 0.231 \pm 0.010$. The asymmetry result is consistent with a recent measurement[30].

[1] $f_d = 0.9^{+0.1}_{-0.2}$, $f_s = 0.02 \pm 0.015$ and $\chi_s = 0.3$ to 0.5 leads to $\chi_{mix} = 0.16 \pm 0.08$. Uncertainties on χ_{mix} arise mainly from the knowledge of χ_d.

	correction
$\sqrt{(s)} \neq M_Z$	- 0.0030
QED initial state	+ 0.0090
QED final state	+ 0.0001
QCD final state	+ 0.0019
γ exchange and interference	- 0.0007

Table 5: corrections to the measured c quark asymmetry.

6 Conclusions

The production of charm quarks at the Z resonance has been studied through charmed meson production. The production rates are measured to be

$$\frac{\Gamma(Z \rightarrow D^{*\pm}X)}{\Gamma_{had}} = 0.187 \pm 0.015(\text{exp.}) \pm 0.013(\text{BR}),$$

$$\frac{\Gamma(Z \rightarrow D^{\pm}X)}{\Gamma_{had}} = 0.251 \pm 0.026(\text{exp.}) \pm 0.025(\text{BR}),$$

$$\frac{\Gamma(Z \rightarrow \overset{(-)}{D}{}^0 X)}{\Gamma_{had}} = 0.518 \pm 0.052(\text{exp.}) \pm 0.035(\text{BR}),$$

where the first error is from this analysis and the second comes from the D branching ratios.

The average fraction of the beam energy carried by a D^* meson in a $Z \rightarrow c\bar{c}$ event was found to be :

$$\langle X_E(D^*) \rangle_c = 0.495 \pm 0.011(\text{stat.}) \pm 0.007(\text{syst.})$$

where the systematic uncertainty takes into account the fragmentation model dependence.

Decays of $D_1(2420)^0$ and/or $D_2^*(2460)^0$ into $D^*\pi$ have been seen. A fraction $(18 \pm 5 \pm 2)\%$ of the $D^{*\pm}$'s is found to come from a D^{**0} decay. Indirect evidence for the production of such heavier states is also found from the apparent low value of the V/V+P ratio 0.51 ± 0.04 obtained from comparing the D^*, D^0 and D^+ rates.

A measurement of the c quark forward-backward pole asymmetry was performed on a subsample enriched with D^* candidates originating from a primary c quark, giving :

$$A_{FB}^{0,c} = 7.7 \pm 4.4\%.$$

Acknowledgement

We wish to thank our colleagues in the CERN accelerator divisions for operating the LEP storage ring. We are grateful to the engineers and technicians in all our institutions for their contribution towards ALEPH's success. Those of us from non-member countries thank CERN for its hospitality.

References

[1] D. Buskulic *et al.* (ALEPH Collab.), Phys. Lett. B 307 (1993) 194.
P. Abreu *et al.* (DELPHI Collab.), Phys. Lett. B 312 (1993) 181.
P. D. Acton *et al.* (OPAL Collab.), Phys. Lett. B 307 (1993) 247.

[2] D. Buskulic *et al.* (ALEPH Collab.), 'Heavy Flavour Production and Decay with Prompt Leptons in the ALEPH Detector', in preparation.

[3] D. Decamp *et al.* (ALEPH Collab.), Phys. Lett. B 266 (1991) 218.

[4] D. Decamp *et al.* (ALEPH Collab.), Nucl. Instrum. Methods A 294 (1990) 121.

[5] G. Batignani *et al.*, Conference Record of the 1991 IEEE Nuclear Science Symposium, 1991, Santa Fe, New Mexico, USA.

[6] W. Atwood *et al.*, Nucl. Instrum. Methods A 306 (1991) 446.

[7] W. Wiedenmann, Nucl. Instrum. Methods A 323 (1992) 213.

[8] D. Decamp *et al.* (ALEPH Collab.), Z. Phys. C – Particles and Fields 53 (1992) 1.

[9] T. Sjöstrand and M. Bengtsson, Comput. Phys. Commun. 46 (1987) 43.

[10] D. Buskulic *et al.* (ALEPH Collab.), Z. Phys. C – Particles and Fields 55 (1992) 209.

[11] C. Peterson, D. Schlatter, I. Schmitt and P. M. Zerwas, Phys. Rev. D 27 (1983) 105.

[12] ALEPH Collab., 'Heavy Flavour Physics with Leptons', Contributed paper to the XXVIth International Conference on High Energy Physics Held in Dallas, Texas, August 6-12, 1992, AIP Conference Proceedings, Ed. R. Schwitters, New York, 1993.

[13] V.G. Kartvelishvili *et al.*, Phys. Lett. B 78 (1978) 615; Yad. Fiz. 38 (1983) 1563.

[14] P. Collins and T. Spiller, J. Phys. **G 11** (1985) 1289.

[15] S. Stone, talk presented at the 5th International Symposium on Heavy Flavour Physics, Montreal, July 6-10, 1993.
M. Thulasidas, 'Hadronic Transitions between $b\bar{b}$ Quarkonia and Measurement of Inclusive Spectra in B Decays'; thesis submitted in Syracuse University (August 1993).

[16] D. Buskulik *et al.*, (ALEPH Collab.), Phys. Lett. B 313 (1993) 549.

[17] Jets are reconstructed with the scaled-invariant-mass clustering algorithm [18].

• variable 1 is the sum of the squared transverse momenta of the particles in the jet with respect to the jet axis of the most energetic jet in the hemisphere [19].
• variable 2 is the momentum of the leading particle of the most energetic jet with respect to the jet axis in the hemisphere [19].
• variable 3 is the boosted sphericity ($\beta_{boost} = 0.965$) of the most energetic jet in the hemisphere.

• variable 4 is the product of the sum of the transverse momenta by the sum of the longitudinal momenta normalized to P^2_{total}.
• variable 5 is the invariant mass of the three most energetic particles in the most energetic jet in the hemisphere [20].
• variable 6 to 9 are the directed sphericities described in [20].

[18] W. Bartel *et al.* (JADE Collab.), Z. Phys. C 33 (1986) 23.

[19] P. Henrard, University of Clermont-Ferrand preprint PC/CF RI 88-08.

[20] L. Bellantoni, J. S. Conway, J. E. Jacobsen, Y. B. Pan and Sau Lan Wu, Nucl. Instrum. Methods A310 (1991) 618.

[21] T. Butler *et al.* (CLEO Collab.), Phys. Rev. Lett. 69 (1992) 2041.

[22] Particle Data Group, Phys. Rev. D 45 (1992).

[23] H. Albrecht *et al.* (ARGUS Collab.), Phys. Rev. Lett. 56 (1986) 549.
J. C. Anjos *et al.* (Tagged Photon Collab.), Phys. Rev. Lett. 62 (1989) 1717.
H. Albrecht *et al.* (ARGUS Collab.), Phys. Lett. B 221 (1989) 422.
H. Albrecht *et al.* (ARGUS Collab.), Phys. Lett. B 232 (1989) 398.
P. Avery *et al.* (CLEO Collab.), Phys. Rev. D 41 (1990) 774.

[24] P. Abreu *et al.* (DELPHI Collab.), 'A measurement of D Meson Production in Z^0 Hadronic Decays', CERN PPE/93-70.

[25] F. Hinode *et al.* (VENUS Collab.), Phys. Lett. B 313 (1993) 245.

[26] M. Artuso *et al.* (CLEO Collab.), Phys. Rev. Lett. 62 (1989) 2233.
H. Albrecht *et al.* (ARGUS Collab.), Phys. Lett. B 192 (1987) 245.

[27] D. Decamp *et al.* (ALEPH Collab.), Phys. Lett. B 258 (1991) 236.

[28] M. Martinez *et al.* Z. Phys. C 49 (1991) 645.

[29] G. Altarelli and B. Lampe, Nucl. Phys. B 391 (1993) 3.

[30] R. Akers *et al.* (OPAL Collab.), 'A measurement of the Forward-Backward Asymmetry of $e^+e^- \rightarrow c\bar{c}$ and $e^+e^- \rightarrow b\bar{b}$ at Centre of Mass Energies on and near the Z Peak Using $D^{*\pm}$', CERN-PPE/93-149 (1993), submitted to Z. Phys. C.

Figure Captions

Fig. 1. $K\pi$ invariant mass distribution, for $X_E(K\pi) > 0.25$. for 1991 data (points with error bars) compared with the fit described in the text. Dotted line: combinatorial background; dashed line: charmed background; solid line: total background and signal including the double counting. The arrows indicate the selection cuts.

Fig. 2. Mass-difference distribution, for $X_E(K\pi\pi) > 0.25$. The $K\pi$ mass is required to be between 1.835 and 1.895 GeV/c^2. The background, calculated by the event-mixing technique, is shown. The solid line shows the sum of the background obtained by event mixing and the signal shape predicted by Monte Carlo normalized to the total number of signal events.

Fig. 3. Fish-eye view of an event containing a high energy $D^{*+} \rightarrow D^0\pi_s^+$ candidate, with the D^0 decaying into $K\pi$. The decay tracks are marked.

Fig. 4. $K\pi\pi$ invariant mass distribution, showing the $D^{\pm}$ signal. The solid line shows the sum of the background (dotted line) and the expected signal shape predicted by Monte Carlo normalized to the total number of signal events.

Fig. 5. $X_E(D^*)$ distribution, as measured separately for $b\bar{b}$ and $c\bar{c}$ events. The solid lines are the Monte Carlo expectations with the parameters extracted from the fit described in Section 4.2.

Fig. 6. a) $X_E(D^*)$ distribution, b) $V_{NN}(D^*)$ distribution, corrected for efficiency and background subtracted. The data are represented by dots with error bars; the best fit is shown (solid line), together with $b\bar{b}$ and $c\bar{c}$ contributions.

Fig. 7. $D^{*\pm}\pi^{\mp}$ effective mass distribution, together with the fitted signal of D^{**}.

Fig. 8. Mass-difference distribution, for the process $D^{*+} \rightarrow D^0\pi_s^+$, $D^0 \rightarrow K^-\pi^+\pi^+\pi^-$. The $K\pi\pi\pi$ mass is required to be between 1.835 and 1.895 GeV/c^2 and $X_E(D^*) > 0.5$. The background (dash-dotted line) is obtained from the upper side band of the $K\pi\pi\pi$ mass distribution. The solid line shows the Monte Carlo simulation.

Fig. 9. $K\pi\pi^0$ invariant mass distribution, for $D^{*\pm}$ candidates with ΔM between 0.1435 and 0.1475 MeV and $X_E > 0.5$. The solid line is a fit of a polynomial for the background plus a gaussian for the signal, to guide the eye.

Fig. 10. Distribution of the signed cosine angle of the $D^{*\pm}$ corrected for efficiency and background subtracted, compared with the angular distribution of charmed quark corresponding to the measured asymmetry.

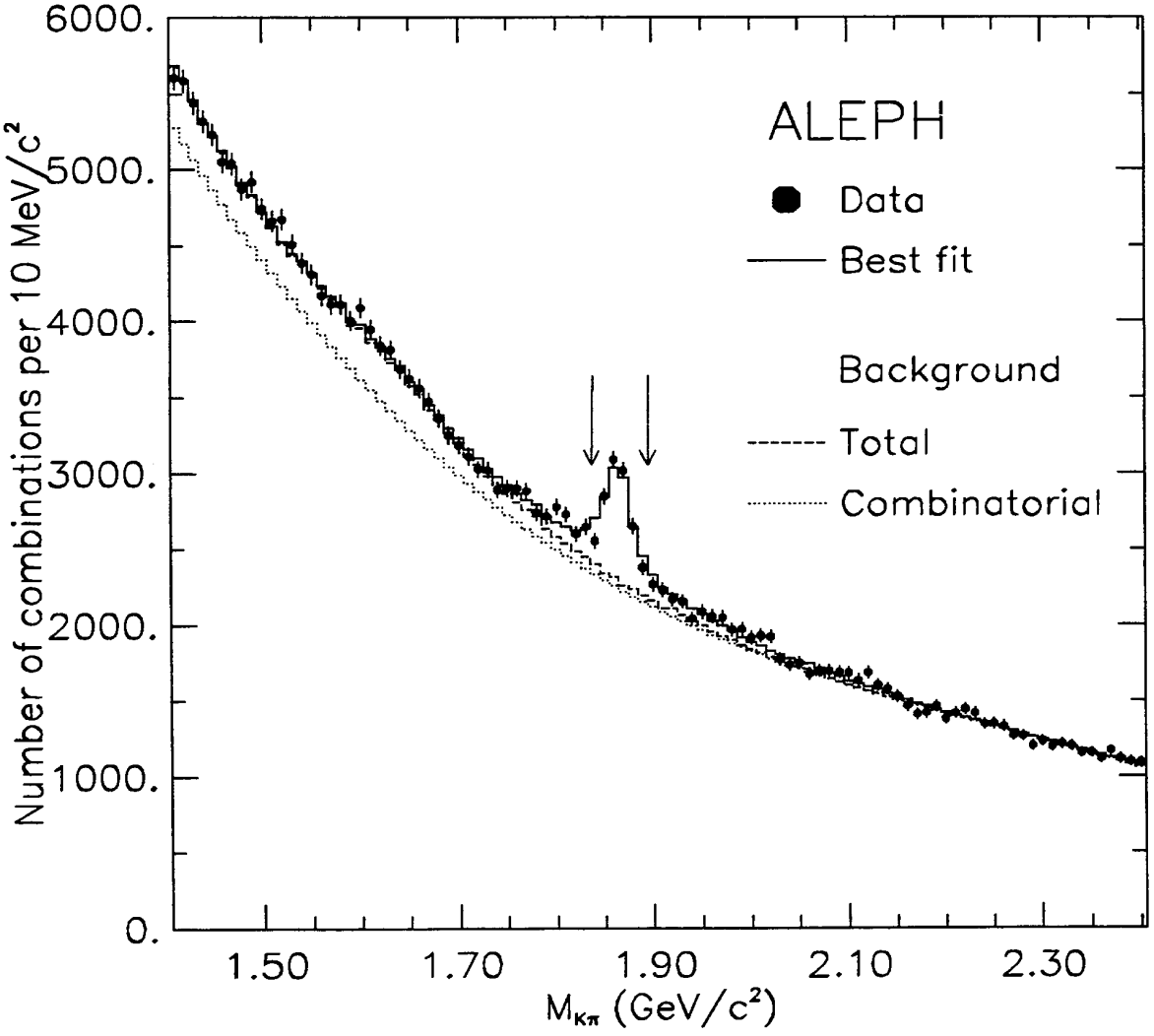
ALEPH
Data
Best fit
Background
Total
Combinatorial
Number of combinations per 10 MeV/c²
6000.
5000.
4000.
3000.
2000.
1000.
0.
1.50
1.70
1.90
2.10
2.30
M_Kπ (GeV/c²)

Figure 1

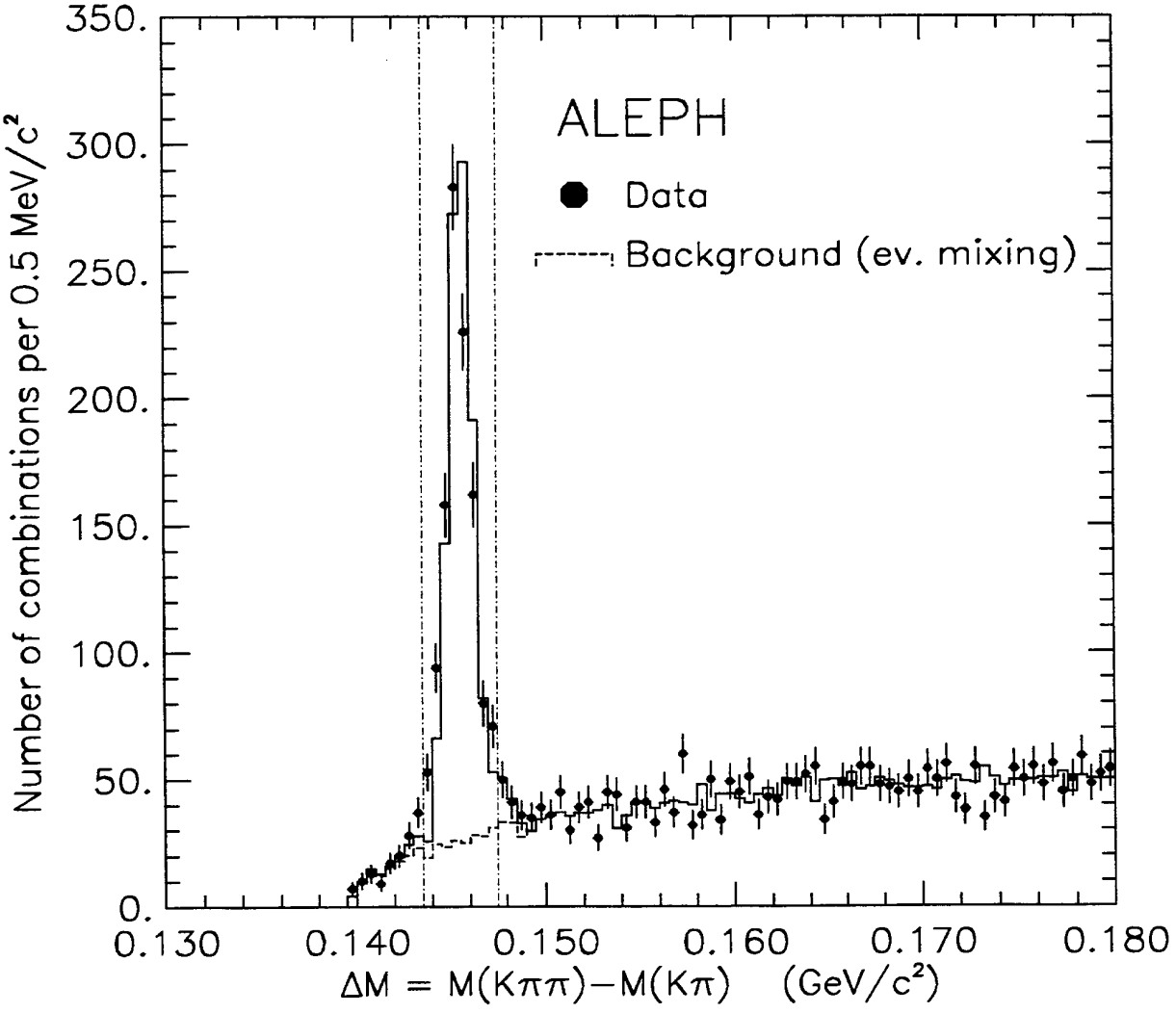
ALEPH
Data
Background (ev. mixing)
Number of combinations per 0.5 MeV/c²
ΔM = M(Kππ)−M(Kπ) (GeV/c²)
350.
300.
250.
200.
150.
100.
50.
0.
0.130
0.140
0.150
0.160
0.170
0.180

Figure 2

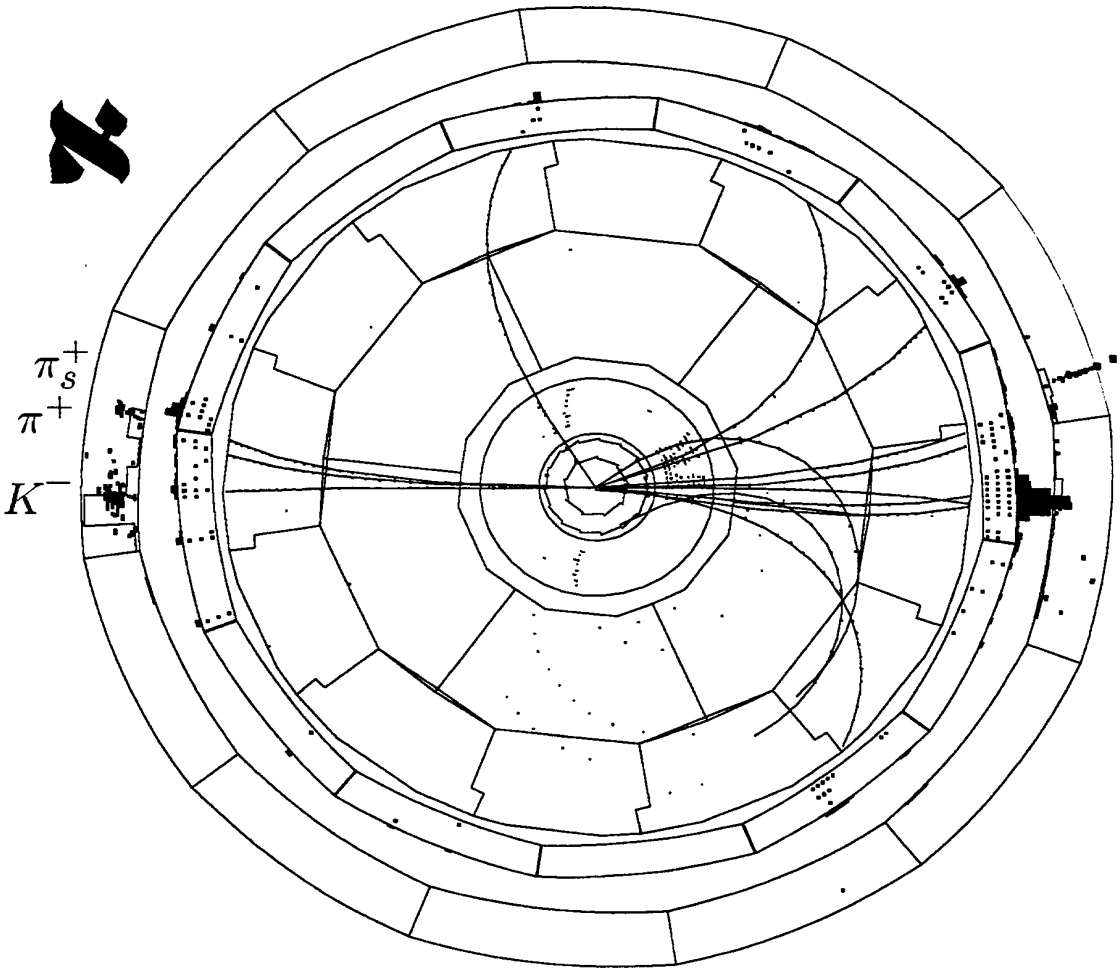

Figure 3

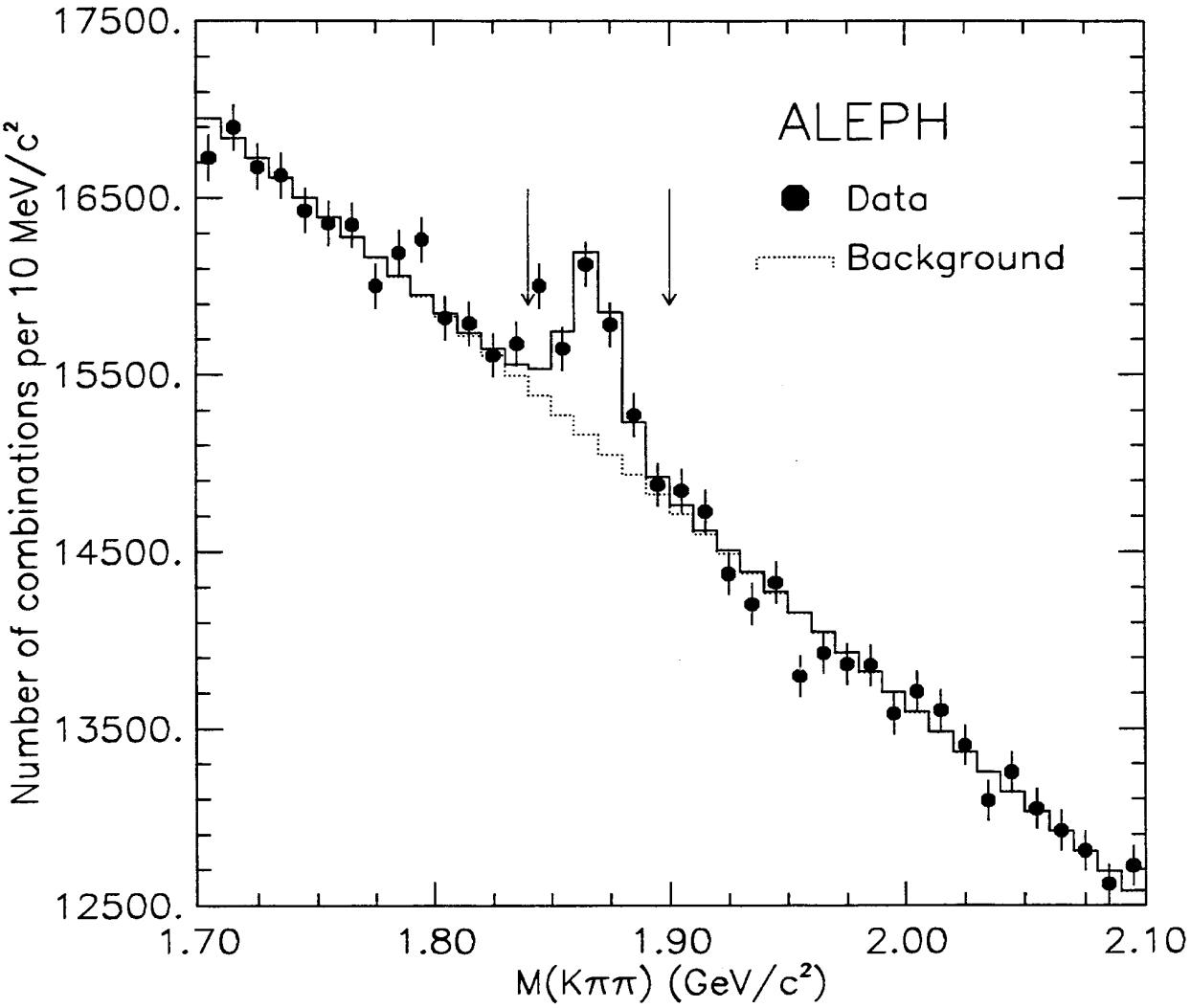
ALEPH
Data
Background
Number of combinations per 10 MeV/c²
17500.
16500.
15500.
14500.
13500.
12500.
1.70
1.80
1.90
2.00
2.10
M(Kππ) (GeV/c²)

Figure 4

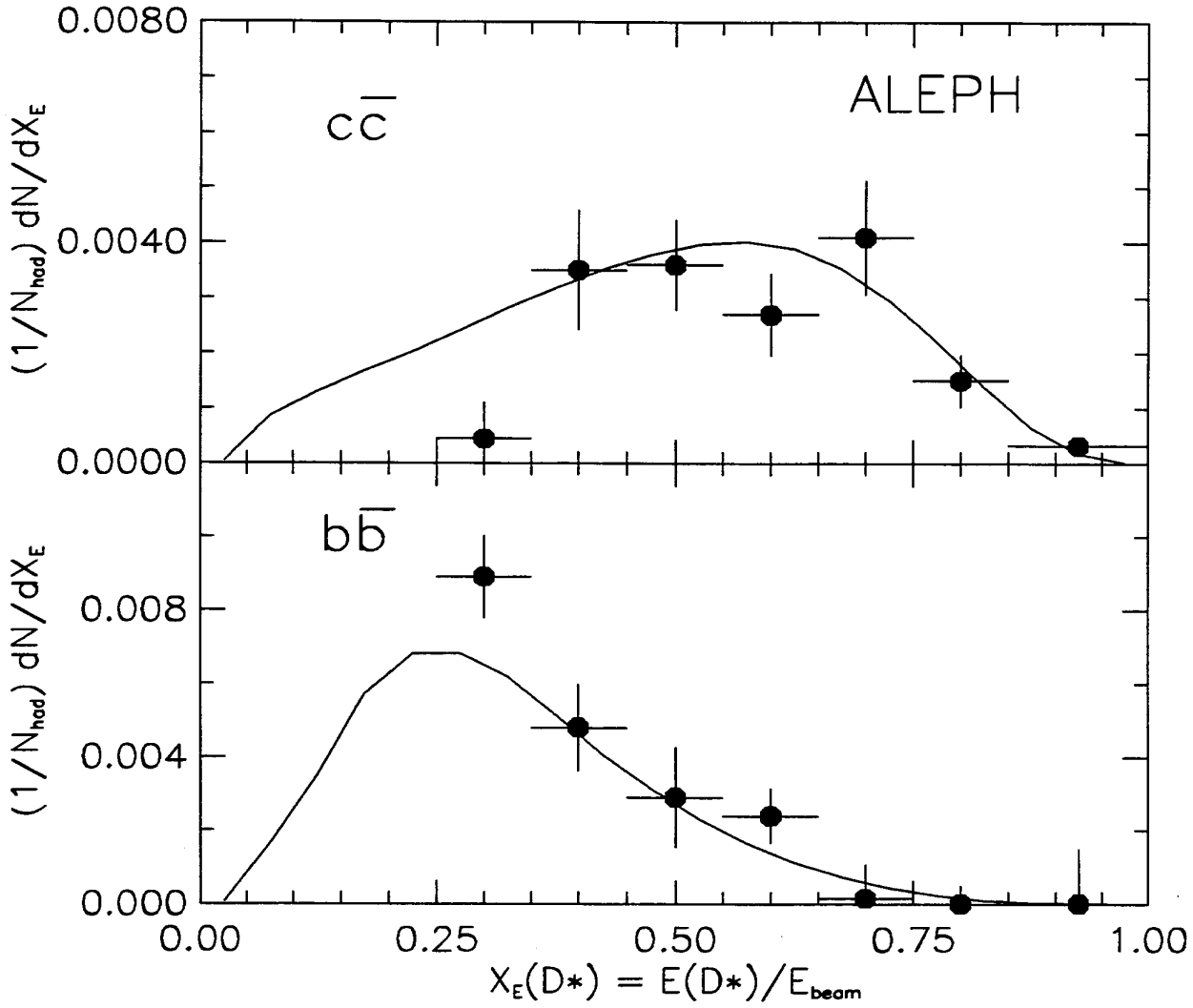
ALEPH
$c\bar{c}$
$b\bar{b}$
$(1/N_{had})\ dN/dX_E$
0.0080
0.0040
0.0000
0.008
0.004
0.000
0.00
0.25
0.50
0.75
1.00
$X_E(D*) = E(D*)/E_{beam}$

Figure 5

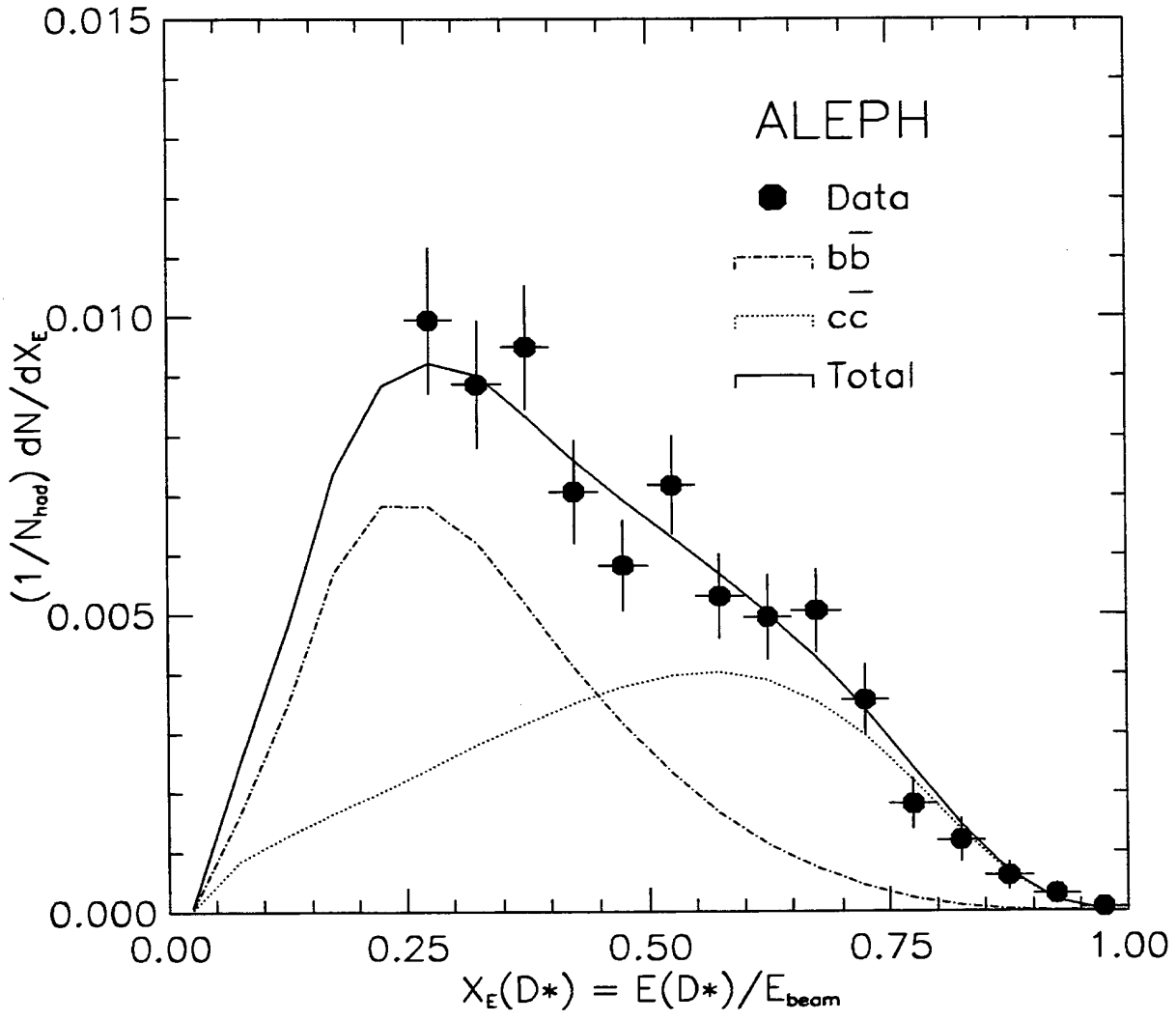
ALEPH
Data
bb̄
cc̄
Total
0.015
0.010
0.005
0.000
0.00
0.25
0.50
0.75
1.00
(1/N_had) dN/dX_E
X_E(D*) = E(D*)/E_beam

Figure 6a

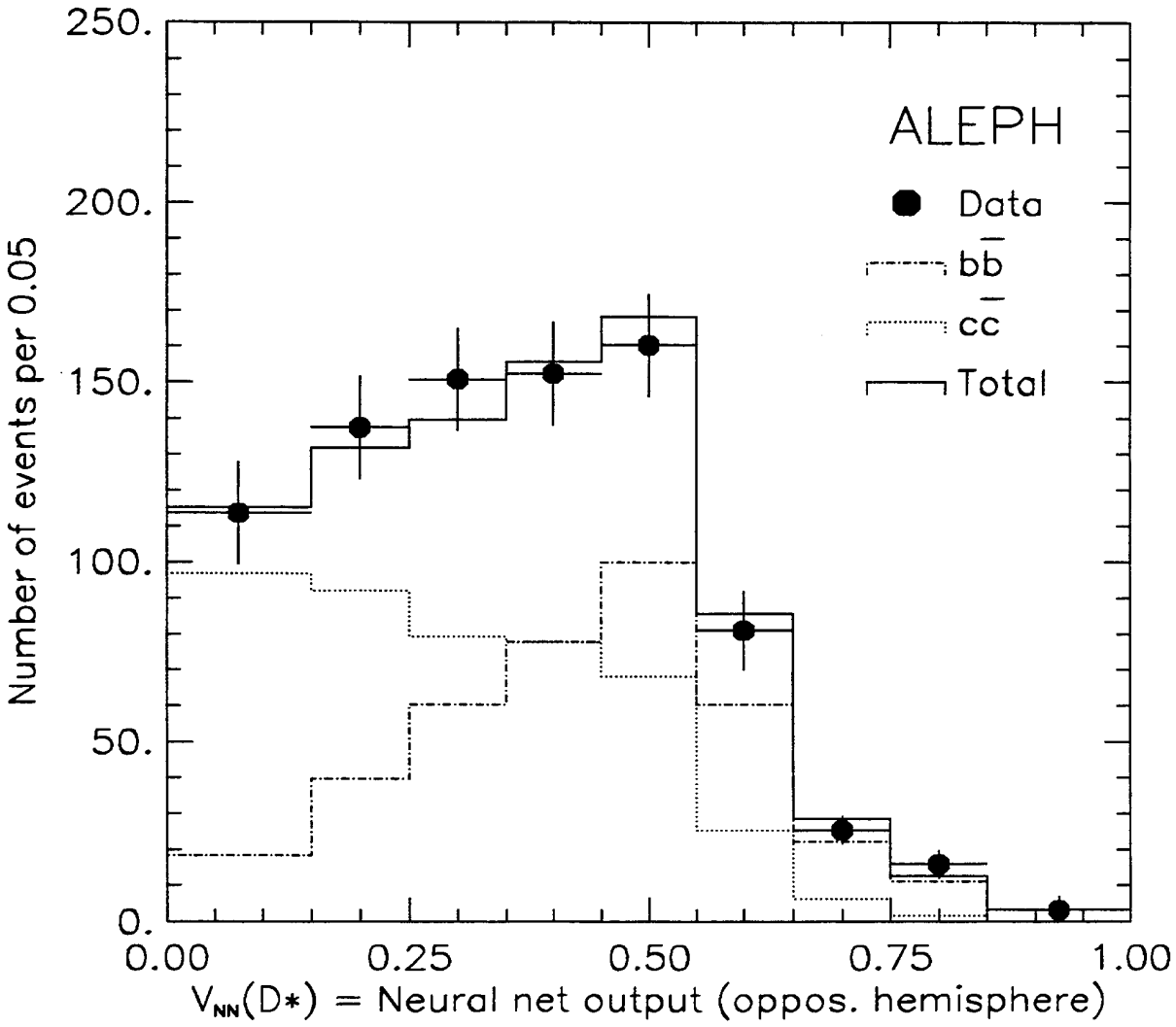
ALEPH
Data
bb̄
cc̄
Total
Number of events per 0.05
250.
200.
150.
100.
50.
0.
0.00
0.25
0.50
0.75
1.00
V_NN(D*) = Neural net output (oppos. hemisphere)

Figure 6b

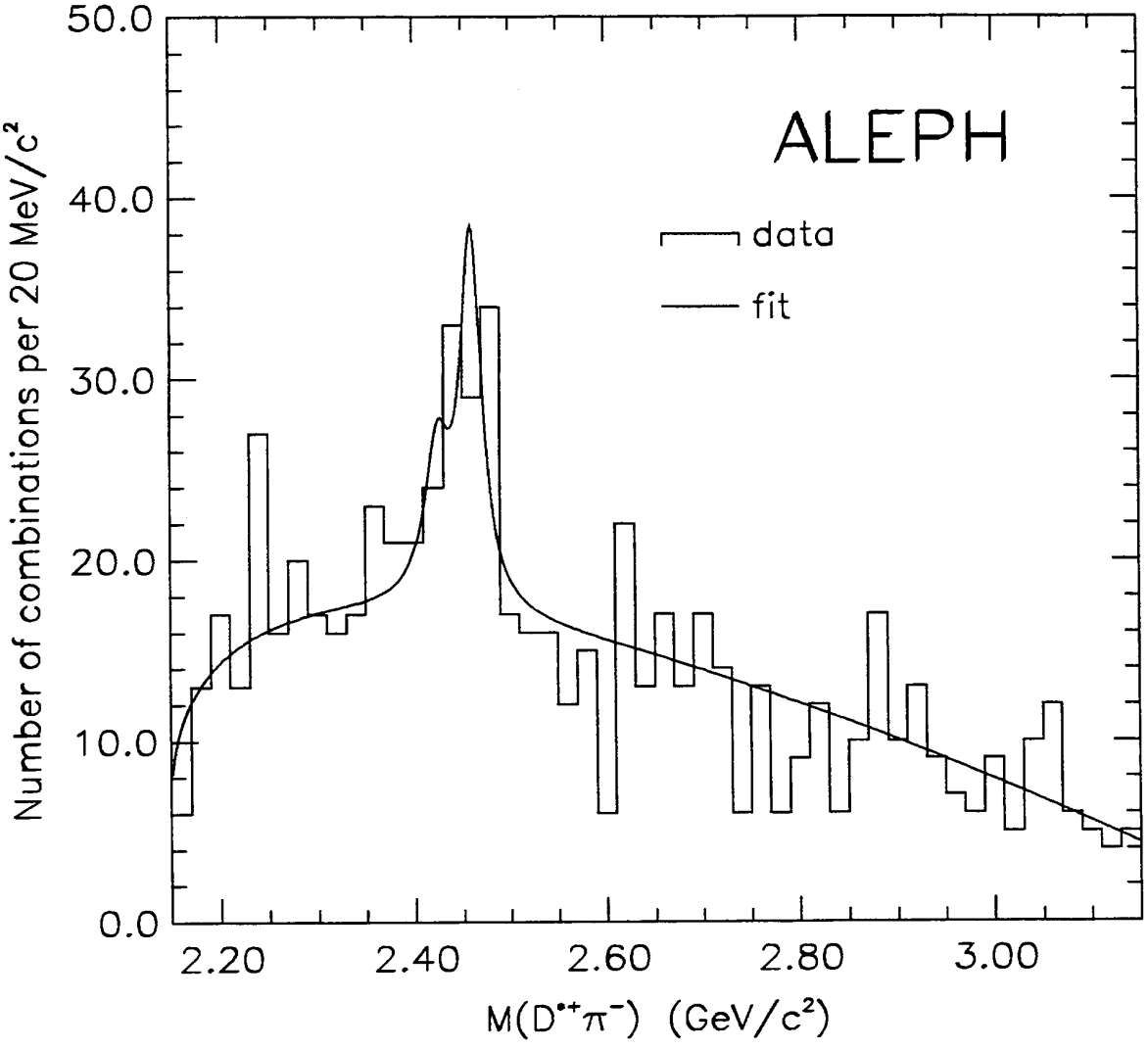
ALEPH
data
fit
50.0
40.0
30.0
20.0
10.0
0.0
2.20
2.40
2.60
2.80
3.00
Number of combinations per 20 MeV/c²
M(D*⁺π⁻) (GeV/c²)

Figure 7

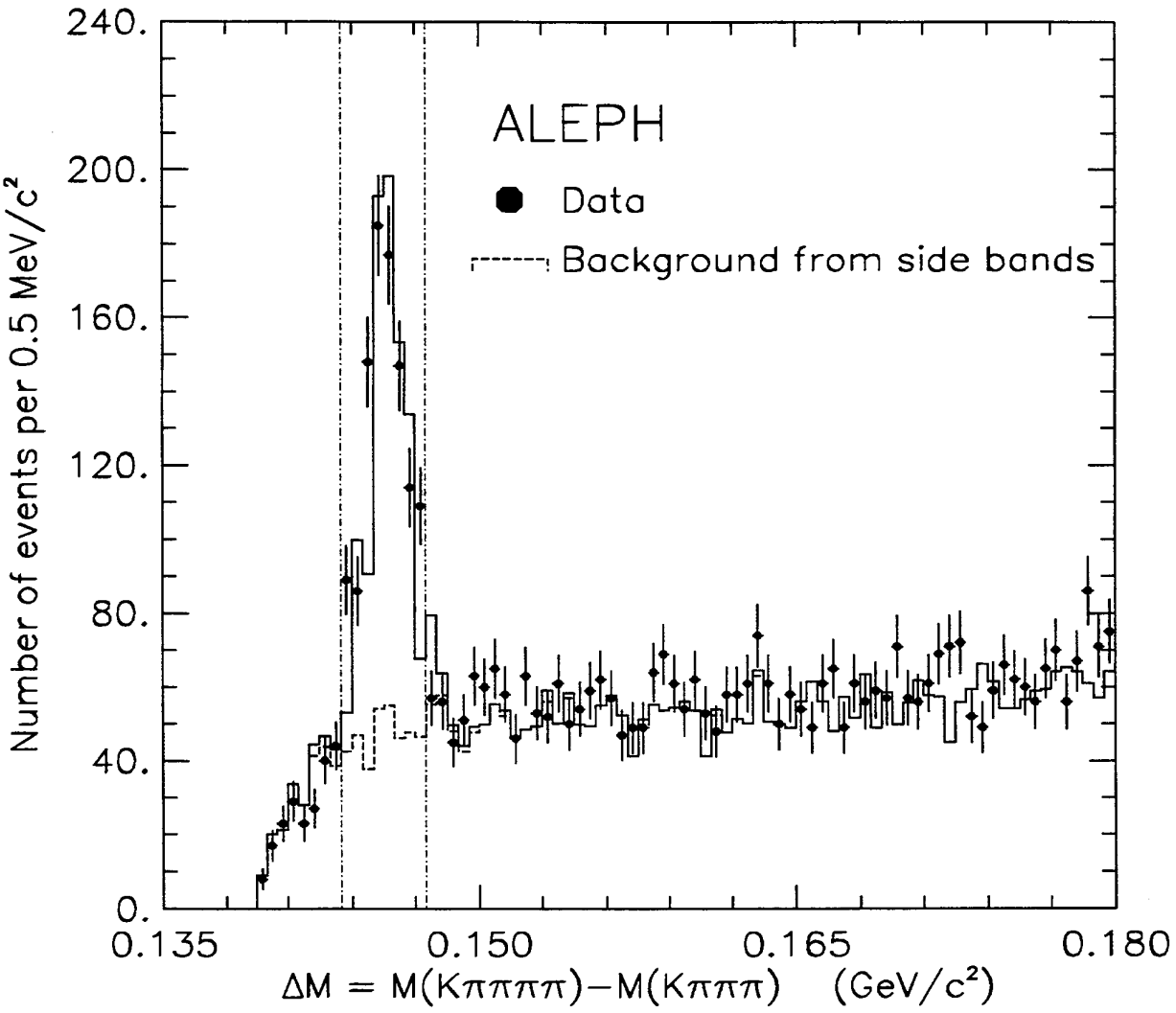
ALEPH
Data
Background from side bands
Number of events per 0.5 MeV/c²
240.
200.
160.
120.
80.
40.
0.
0.135
0.150
0.165
0.180
ΔM = M(Kπππ)−M(Kππ) (GeV/c²)

Figure 8

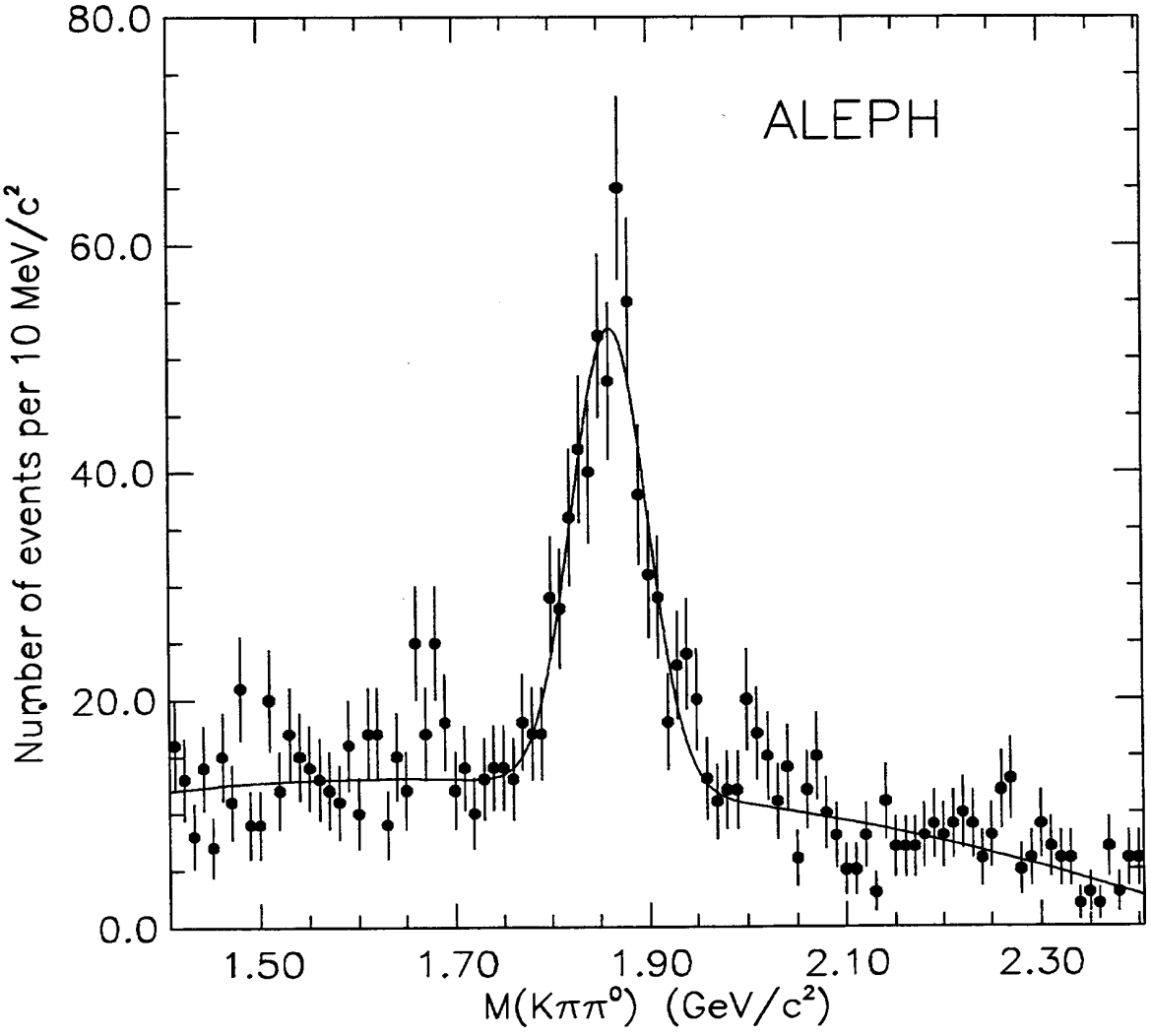
ALEPH
80.0
60.0
40.0
20.0
0.0
Number of events per 10 MeV/c²
1.50
1.70
1.90
2.10
2.30
M(Kππ°) (GeV/c²)

Figure 9

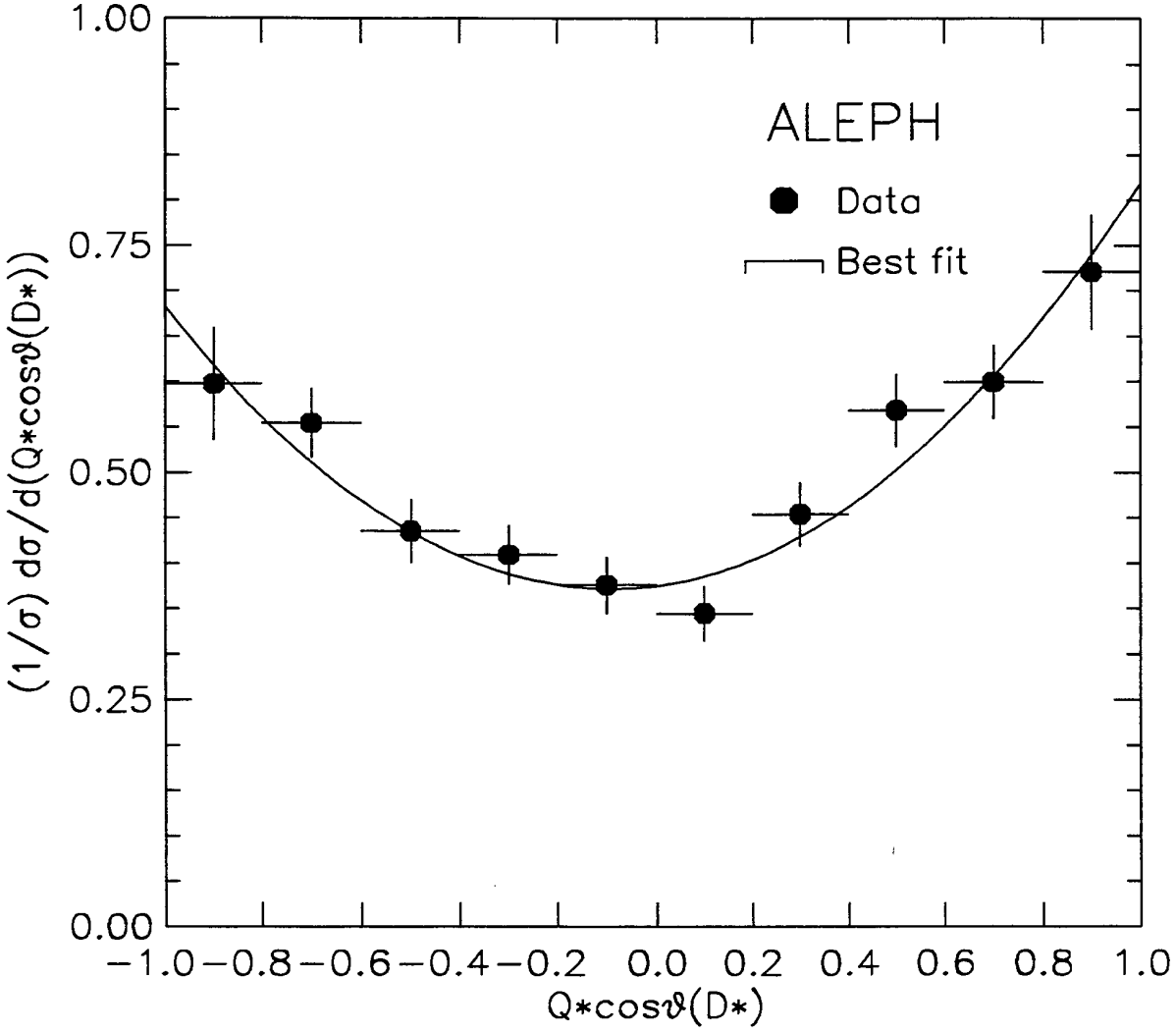
ALEPH
Data
Best fit
1.00
0.75
0.50
0.25
0.00
−1.0 −0.8 −0.6 −0.4 −0.2 0.0 0.2 0.4 0.6 0.8 1.0
(1/σ) dσ/d(Q*cosϑ(D*))
Q*cosϑ(D*)

Figure 10